Tucholke, B.E., Sibuet, J.-C., and Klaus, A. (Eds.)
Proceedings of the Ocean Drilling Program, Scientific Results Volume 210

2. Petrology and Provenance of Eocene–Albian Sandstones and Grainstones Recovered during ODP Leg 210: Implications for Passive Margin (Rift-to-Drift) Sandstone Provenance Models[1]

Kathleen M. Marsaglia,[2] Jennifer A. Pavia,[2] and Sara J. Maloney[2]

ABSTRACT

Sand detrital modes of Albian–Eocene clastic gravity-flow deposits cored and recovered at Ocean Drilling Program Site 1276 reflect the postrift geologic evolution of the Newfoundland passive continental margin. Cretaceous sandstone compositions (average: $Q_{57}F_{23}L_{20}$; Ls%Lsc = 35; total%bioclasts = 3) are consistent with a source on Grand Banks such as Avalon Uplift. Their relatively low potassium feldspar ($Qm_{71}K_8P_{21}$) contents distinguish them from Iberian sandstones and appear to preclude an easterly source during the early history of the ocean basin. Isolated volcaniclastic input near the Paleocene/Eocene boundary (~60 Ma) at Site 1276 is also present in Iberian samples of this age, suggesting that magmatism was widespread across the North Atlantic during this time frame; the source(s) of this volcanic debris remains equivocal. In the Eocene, the development of carbonate bank facies on the shelf marks a profound compositional change to calcareous grainstones (average: $Q_{27}F_{11}L_{62}$; Ls%Lsc = 82; total%bioclasts = 55) in basinal gravity-flow deposits at Site 1276. This calcareous petrofacies is present on the Iberian margin and in the Pyrenees, suggesting that it was a regional event. The production and downslope redistribution of carbonate

[1]Marsaglia, K.M., Pavia, J.A., and Maloney, S.J., 2007. Petrology and provenance of Eocene–Albian sandstones and grainstones recovered during ODP Leg 210: implications for passive margin (rift-to-drift) sandstone provenance models. *In* Tucholke, B.E., Sibuet, J.-C., and Klaus, A. (Eds.), *Proc. ODP, Sci. Results,* 210: College Station, TX (Ocean Drilling Program), 1–47. doi:10.2973/odp.proc.sr.210.107.2007
[2]Department of Geological Sciences, California State University, Northridge CA 91330-8266, USA. Correspondence author: **kathie.marsaglia@csun.edu**

Initial receipt: 13 January 2006
Acceptance: 31 August 2006
Web publication: 18 June 2007
Ms 210SR-107

debris, including bioclastic and lithic fragments, was likely eustatically controlled.

The Newfoundland (Site 1276 and Jeanne d'Arc Basin) sandstones are mainly quartzolithic. Their composition and the contrast in composition between them and more quartzofeldspathic sandstones from the Iberian margin are likely a product of rifting along a Paleozoic suture zone separating distinct basement terranes. This prerift geologic setting contrasts with that of rifts developed within other cratonic settings with variable amounts of synrift volcanism. When synthesized, the spectrum of synrift and postrift sand compositions produces a general model of passive margin (rift-to-drift) sandstone provenance.

INTRODUCTION

Ocean Drilling Program (ODP) Site 1276 is located on the eastern flank of Grand Banks, south of Flemish Cap in 4565 m of water (Fig. F1) (Tucholke, Sibuet, Klaus, et al., 2004). At this site, 800 m of Oligocene–Quaternary section was drilled and cased prior to rotary coring from 800 to 1736.9 meters below seafloor. The recovered section, as summarized in Figure F2, is mainly hemipelagic mudrocks, generally noncalcareous bioturbated claystone, and mudstone deposited below the carbonate compensation depth (>2000 m water depth), with variable proportions of interbedded gravity-flow deposits. The latter are complex mixtures of terrigenous and calcareous components ranging from mudstone to marlstone and sandstone to grainstone. Shipboard scientists divided the postrift Oligocene–Albian section into five units based on their composition, texture, and sedimentary structures (Fig. F2).

The major purpose of this first deep test of the Newfoundland margin, to recover basement and rift-related sediments (see the *Leg 210 Scientific Prospectus* [www-odp.tamu.edu/publications/prosp/210_prs/210toc.html]), was prevented by the presence of an alkaline diabase sill complex within the Albian section (Fig. F2). Nevertheless, the quantity and variety of sandy gravity-flow deposits recovered during ODP Leg 210 was surprising. Furthermore, the recovery rate was excellent (85% of ~1000 m cored) (Fig. F2), meaning that these cores constitute a nearly continuous record of sedimentation on this segment of the Newfoundland margin, which makes them superb candidates for providing insight into the regional paleogeographic evolution of the northern Atlantic Ocean and for comparing and contrasting the sedimentological and tectonic evolution of the Iberia–Newfoundland conjugate margin pair. Owing to the presence of unstable formations and associated drilling problems, logging was not possible during Leg 210 (Tucholke, Sibuet, Klaus, et al., 2004) and therefore paleocurrent data (e.g., orientation via formation microscanner logs) are not available. This placed added emphasis on sediment (sand) composition in evaluating sediment sources and dispersal pathways for paleogeographic reconstructions of this margin. This study provides quantitative data on the percentages of components within sandy gravity-flow deposits, as well as authigenic phases, and porosity for the purposes of establishing downhole trends and comparison to exploration wells on the shelf, as well as to prior Deep Sea Drilling Project (DSDP) and ODP sites on the conjugate Iberian margin (e.g., Marsaglia et al., 1996). These combined data sets are used to construct a general model of sand provenance on rifted continental margins.

F1. Bathymetric map of Leg 210 sites, p. 16.

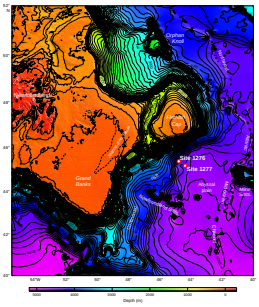

F2. Summary stratigraphic column for Hole 1276A, p. 17.

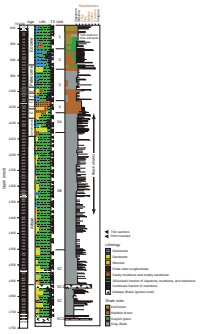

SAMPLE AND DATA SETS

At Site 1276, one sample was collected shipboard per sand-bearing core, except where sandstones with different compositions or diagenetic states were encountered within a given core, or in the case of a unique facies, such as the volcaniclastic-bearing interval in the middle Paleocene (Core 210-1276A-15R). A total of 114 mostly fine to very fine grained sandstone samples were collected from Site 1276 cores. One aim of this study was to compare sand detrital modes across conjugate passive margins. Significant parallels between the section recovered at Site 1276 and that cored at Site 398 near Galicia Bank on the Iberian margin were outlined by Leg 210 shipboard scientists (Tucholke, Sibuet, Klaus, et al., 2004), but there were no published petrographic data for these cores. Thus, for comparison with the Iberian margin, an additional 45 samples of Eocene–Hauterivian gravity-flow deposits from DSDP Site 398 (Galicia Bank) cores (Sibuet, Ryan, et al., 1979; Shipboard Scientific Party, 1979) were collected at the ODP East Coast Core Repository at Lamont-Doherty Earth Observatory for analysis in this study (Figs. F3, F4). A total of 80 shipboard-prepared thin sections from Mesozoic sandy intervals recovered from Holes 1065A and 1069A during Leg 173 (Fig. F4) were reviewed, and several samples were chosen to point count, providing additional Jurassic and Cretaceous data sets. Thin sections and sand detrital modes (50 samples) from Leg 149 (Marsaglia et al., 1996) were available for use in this study (Fig. F4). Samples from lower Paleocene (~60 Ma) intervals on the Iberian margin were also reviewed to check for evidence of volcanism. Data sets or descriptions were also used from Legs 103 (31 Aptian and older samples; Johnson, 1988) and 173 (lower Eocene–Campanian; Wallrabe-Adams, 2001), as well as petroleum data from the shelf (e.g., Hesse and Abid, 1998). Additional unpublished petroleum company data made available by Petro-Canada (Wilson and Webb, unpubl. data [N1]) provide some information on Tithonian–Albian producing horizons from within and around the Jeanne d'Arc Basin in the Grand Banks area (Fig. F1). The latter data were collected from thin sections of core as well as drill cuttings of sandstone formations.

METHODS

Thin sections were prepared from the 114 samples from Site 1276, as well as from 45 samples taken from DSDP Site 398 (Galicia Bank). Samples were first high-pressure vacuum-impregnated with blue-dyed epoxy for porosity recognition (Fig. F5). Then standard thin sections were prepared and stained for easy recognition of potassium and calcium feldspar (Fig. F6) using the technique outlined in Marsaglia and Tazaki (1992). Preliminary petrographic analysis showed that many of the Site 398 and 1276 samples were unsuitable for point counting, owing to insufficient sand-sized detritus. Samples were selected for point counting based on their location in the sections and their sand content; these are located on Figures F2 and F3. Thin sections prepared shipboard during Leg 173 were obtained from ODP and petrographically examined; some were selected for point-count analysis. Note that these thin sections were not stained for feldspar recognition. Compositional modes were determined using a Swift automated stage and point counter in the manner outlined by Marsaglia et al. (1996). As many as 400 grains were counted for each sample, in part a function of sand size and density

F3. Stratigraphic column for DSDP Site 398, p. 18.

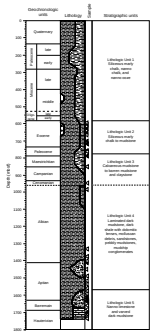

F4. Reconstruction of the Newfoundland–Iberia conjugate margins at 121 Ma, p. 19.

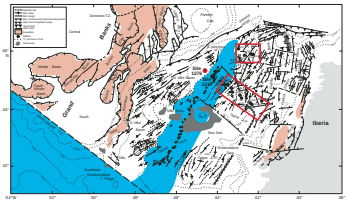

F5. Photomicrographs of Sample 210-1276A-9R-5, 118 cm, p. 20.

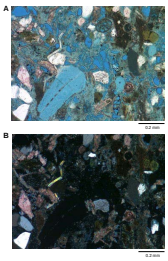

F6. Photomicrographs of Sample 210-1276A-49R-2, 130 cm, p. 21.

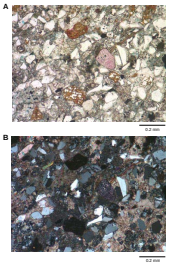

within a sample, with additional points tallied for porosity, matrix, and interstitial cements. The mixed nature of these gravity-flow deposits required a mix of techniques and categories: those for siliciclastic petrofacies and provenance studies (e.g., Ingersoll, 1990; Ingersoll et al., 1984), as well as for carbonate microfacies (e.g., Carozzi, 1989). Counted categories are presented in Table AT1 (see "Appendix," p. 15).

RESULTS

Petrographic data for the counted samples are presented in Table AT2 (see "Appendix," p. 15) and summarized in Table T1 through the use of various recalculated parameters. We review their composition below, grouping them loosely into Cretaceous and Cenozoic categories. Additional information and photomicrographs based on shipboard-prepared thin sections can be found in Tucholke, Sibuet, Klaus, et al. (2004).

The dominant component of the Cretaceous sandstone samples is monocrystalline quartz (Fig. F6). Polycrystalline quartz is minor. Feldspar is common, with plagioclase often more prevalent than potassium feldspar. These sandstones exhibit a significant range in the proportion of metamorphic (including metasedimentary) (Figs. F7, F8) and sedimentary lithic fragments. In decreasing order of importance, the metamorphic lithic fragments consist of quartz-mica tectonite, polycrystalline mica, and quartz-feldspar-mica aggregates, where the mica (platy mineral) components include muscovite, biotite, and chlorite. Fine-felted phyllite fragments of uncertain mineralogy are also present. Siliciclastic sedimentary lithic fragments are dominated by claystone with traces of feldspathic siltstone and sedimentary chert. Calcareous sedimentary lithic fragments, locally important components, are mainly micritic and microcrystalline carbonate. We could not determine whether these were coeval or noncoeval carbonate particles. Volcanic lithic fragments are rare, generally microlitic with a few exhibiting vitric, lathwork, and felsitic textures. Platy muscovite, biotite, and chlorite fragments (Fig. F7) are rare to minor components. Nonopaque (e.g., zircon, sphene, and tourmaline) and opaque dense minerals are very rare. Glauconite, generally a trace component, is more common in Santonian and younger units. Bioclasts are generally foraminifers, with lesser bryozoan, mollusk, and echinoderm fragments. We did not separate coeval from noncoeval bioclasts because that was the focus of another postcruise study by Georgescu et al. (submitted [N2]). Plant debris is rare. The sandstones are commonly cemented by poikilotopic (Fig. F6) to microcrystalline (Fig. F7) carbonate with traces of authigenic pyrite and gypsum. Silica cement (chert) is often associated with siliceous bioclasts. Rare quartz overgrowths are likely inherited features. Kaolinite cement and/or grain (feldspar?) replacement is present between the sills (Fig. F9). In the carbonate-cemented intervals, porosity is secondary intraparticle, mainly associated with grain dissolution. Primary intraparticle porosity in foraminifers can be locally significant. Interparticle porosity is more important in less cemented intervals in the upper part of the Cretaceous section (e.g., Cores 210-1276A-44R and 25R). Matrix is present in the more poorly sorted samples, and it is locally microporous.

A similar array of terrigenous debris is found in the Cenozoic sandstones/grainstones; however, the siliciclastic components are significantly subordinate to calcareous lithic fragments and bioclasts in these samples. Bioclasts are much more common, with more foraminifers in

T1. Recalculated parameters, p. 38.

F7. Photomicrographs of Sample 210-1276A-81R-3, 134 cm, p. 22.

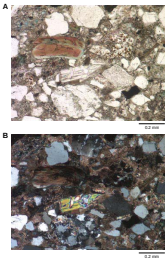

F8. Photomicrographs of Sample 210-1276A-93R-1, 24 cm, p. 23.

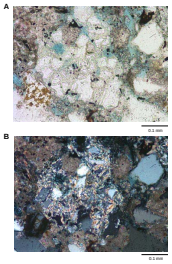

F9. Photomicrographs of Sample 210-1276A-90R-5, 87 cm, p. 24.

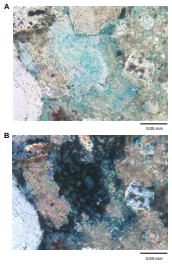

particular, as well as more mollusk fragments. They differ from underlying Cretaceous units in having more benthic foraminifers, fewer echinoderm fragments, and minor amounts of siliceous biogenic debris (radiolarians and sponge spicules), red algae, and phosphatic bone fragments. Glauconite is also present. These samples are either matrix rich or carbonate cemented with generally low porosity but locally high porosity (Fig. F5). The foraminifers are thought to be allochthonous and transported from upslope (Georgescu et al., submitted [N2]; Tucholke, Sibuet, Klaus, et al., 2004). These include planktonic and benthic varieties, partly penecontemporaneous and partly reworked from older units (Georgescu et al., submitted [N2]).

The QFL data displayed in Figures F10, F11, and F12 show the Cenozoic sandstones to have higher lithic proportions than the Cretaceous sandstones at Site 1276. The shift (from more metamorphic) toward more sedimentary lithic fragments with time at Site 1276 is displayed in Figure F13. The sandstones show similar proportions of quartz, plagioclase, and potassium feldspar (Fig. F14).

PROVENANCE OF CRETACEOUS GRAVITY-FLOW DEPOSITS

There appears to be no significant difference in sandstone detrital modes across the Cretaceous section recovered at Site 1276. Grain size can be an indicator of different turbidite sources, with more proximal sources or higher energy sources perhaps providing coarser sediment. Unit 5 contains sandstones that range from very fine to fine to medium grain size. An analysis of the Unit 5 data showed no distinct relationships between grain size and composition. Furthermore, there are also no apparent differences between Subunits 5b and 5c. Hiscott (this volume) describes concentrated muddy or "slurry" flow deposits in Units 3 and 5 that he attributes to slope failures. These have the potential for being of a different provenance than the more classical turbidites in the section. Units 3 and 5 do not have significantly different compositions from the intervening Unit 4 (Table T1). The above relationships tend to point toward one main source of terrigenous sediment at Site 1276 during the Cretaceous.

Several possible sources of sandy material were discussed by the shipboard scientists (Tucholke, Sibuet, Klaus, et al., 2004); they included (1) the continental Newfoundland margin to the southeast (Avalon Uplift) and north (Flemish Cap); (2) the conjugate Iberian margin, which is plausible during the early history when the ocean basin was narrow; and (3) extrabasinal sources from the northern gateway (Greenland via the Labrador Sea). The possibility of northern (strike-parallel) sources is more difficult to address, so we focus our attention on assessing the viability of Newfoundland vs. Iberian margin sources below.

The continental margin of Newfoundland is tectonically complex, having been affected by the Taconian (Ordovician), Acadian (Devonian), and Alleghenian–Hercynian (Permian) orogenies prior to Triassic–Jurassic rifting, which was followed by a period of Cretaceous rifting and seafloor spreading (e.g., Grant and McAlpine, 1990). On the Grand Banks west of Site 1276, Mesozoic sedimentary rocks onlap Paleozoic and Precambrian sedimentary, metasedimentary, and igneous rocks that form two prominent highs: Avalon Uplift and Flemish Cap (Grant and McAlpine, 1990). Rocks encountered by exploration wells on Ava-

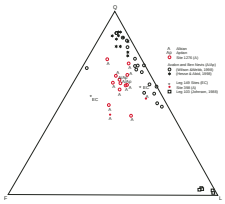

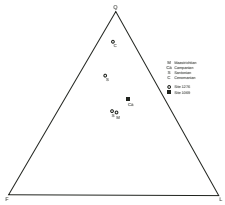

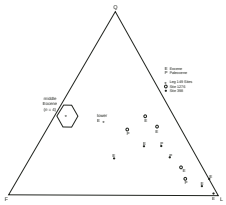

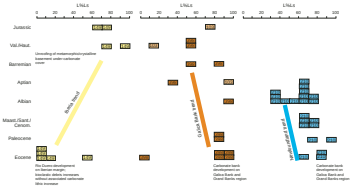

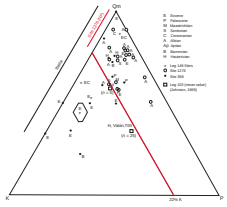

lon Uplift include granite, schist, phyllite, slate, metaquartzite, and greywacke and limited Devonian granite, whereas late Proterozoic granodiorite was encountered on Flemish Cap (see summary in Grant and McAlpine, 1990; Bell and Howie, 1990; Jansa and Wade, 1975). Devonian redbeds and Carboniferous sedimentary rocks have also been encountered on Grand Banks (Bell and Howie, 1990), but no Permian strata have been as yet discovered, which Jansa and Wade (1975) attribute to Hercynian tectonism. The geology of Flemish Cap is largely unknown, making it difficult to assess its potential for sourcing Site 1276 sandstones. Furthermore, the geology may be in part similar to Galicia Bank in that Ziegler (1989) extends Galicia Bank Variscan belt rocks into this region. **Hiscott** (this volume) suggests that from ripple cross-lamination and grain-fabric studies, coupled with recognition of primary dip of reflectors on seismic sections, the likely source of Site 1276 gravity-flow deposits was Avalon Uplift. Luckily, more is known about this high and sand sourced from it on Grand Banks, which allows us to test the source hypothesis posed by **Hiscott** (this volume).

Avalon Uplift is considered to be the major source of sand within Jeanne d'Arc Basin (e.g., Brown et al., 1989). Therefore, sandstone detrital modes from the Jeanne d'Arc Basin can be used to characterize this now submerged Precambrian–Paleozoic source terrain for the purposes of comparison with Site 1276 data. Early Cretaceous sandstone reservoirs discussed in the literature include the Aptian/Albian Ben Nevis Formation, which is partly time equivalent to Unit 5 at Site 1276, but most data come from older formations.

Brown et al. (1989) report that the upper Hibernia very fine to coarse-grained sandstones of earliest Cretaceous (Berriasian) age from the Hibernia Field of Grand Banks are relatively matrix free shallow to marginal marine sandstones thought to have been derived from Avalon Uplift, carried northward by a river that emptied into a tide-dominated delta system. They analyzed ~40 samples and found them to be mature quartz arenites (QFL%Q = 98.7%) with minor albite and potassium feldspar (QFL%F = 1.0; P/F not determined) that has been affected by diagenesis (dissolution/alteration). They interpret multiple sources for the quartz grains: igneous, metamorphic, and recycled sedimentary rocks with abraded quartz overgrowths. The lithic population is limited to a small percentage of shale and sedimentary fragments (QFL%L = 0.3). They are thought to have been derived from the Precambrian, Paleozoic, and younger Mesozoic units known in the area, including Precambrian craton and Paleozoic orogen and older Mesozoic sedimentary rocks. As Brown et al. (1989) did not report their methodology, we did not include these samples on the QFL plots.

Hesse and Abid (1998) provide some compositional data from Hibernia Field sandstones in their diagenetic study. They did not stain for feldspar recognition but counted 500 points per section using traditional counting methods. The dominant component was quartz with minor feldspar and sedimentary lithic fragments. They found only traces of metamorphic, volcanic, and plutonic lithic fragments. Data for samples of the Jeanne d'Arc Formation, Hibernia Formation, and Avalon Sandstone are presented for comparison to Site 1276 in Figures **F10, F15,** and **F16.**

Wilson and Webb (unpubl. data [**N1**]) collected detrital modes of Jurassic–Cretaceous sandstone core and cutting samples from within and to the east of Hibernia Field. They stained the thin sections for feldspar recognition but only counted as many as 200 points per sample. They used traditional methods as opposed to the Gazzi-Dickinson

F15. Ternary QFL plot of Lower Cretaceous sandstone data, p. 30.

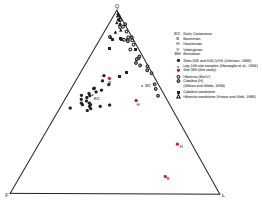

F16. Ternary QFL plot of Tithonian and Jurassic sandstone data, p. 31.

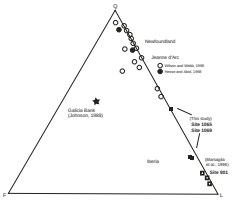

point-counting method used in this study. Intervening units exhibit similar ranges of QFL compositions to those pictured. They found only trace to minor amounts of chert, feldspar, mica, volcanic, and granitic fragments. More common are metamorphic lithic fragments including quartz-mica (muscovite/chlorite) tectonite and metasedimentary rocks and claystone fragments. Rare to common carbonate fragments (bioclasts, micrite, and ooids) are also present. They support an increase in plutonic rock fragments through time, consistent with an unroofing sequence. Their data from the Tithonian Jeanne d'Arc Formation and the Lower Cretaceous Avalon, Ben Nevis, and Eastern Shoals Formations are presented for comparison to Site 1276 data in Figures **F10, F15,** and **F16.**

Variability among these three data sets can be attributed to differences in staining and point-count methodologies, as well as the classification scheme of sedimentary vs. metasedimentary vs. metamorphic lithic fragments. The highly quartzose nature of the Brown et al. (1989) sandstones could in turn be attributable to their depositional environment. Beach and shelf sands can be more mature (quartzose) than fluvial and deep-marine counterparts (e.g., Kairo et al., 1993). From their descriptions, our techniques and data set are most comparable to those of Wilson and Webb (unpubl. data [**N1**]). Overall, the Site 1276 sandstones are similar in composition to the Jeanne d'Arc sandstones. The slightly higher feldspar content of the Site 1276 sands (Fig. **F14**) could be a function of differences in depositional environment (e.g., Kairo et al., 1993) as discussed above or simply a function of grain size. Marsaglia et al. (1996) showed that feldspar could be concentrated in finer-grained turbidites.

Assessing the viability of an Iberian source sand at Site 1276 during the Cretaceous is more difficult. Only a few Lower Cretaceous sandstones from the Iberian margin were analyzed by Marsaglia et al. (1996) because basement highs with thin Cretaceous sections were targeted for drilling. Better age constraints at DSDP Site 398 on the southern flank of Galicia Bank allowed for a few Albian–Aptian sandstones to be identified and point counted for this study. The Site 398 and Leg 149 samples show a similar range of QFL percentages (Fig. **F10**) but group into feldspatholithic and quartzolithic end-members. The latter are similar to contemporaneous Jeanne d'Arc Basin sandstone compositions (Fig. **F10**), and the former are similar to older Leg 103 sandstones derived from Galicia Bank (Fig. **F15**). Site 1276 Albian sandstones exhibit compositions intermediate (Fig. **F10**), being slightly more feldspathic than contemporaneous Jeanne d'Arc Basin sandstones. Monomineralic populations show the Site 1276 sandstones to be slightly less feldspathic, with some of the lowest potassium feldspar proportions. Lithic proportions show similar differences, with the Site 1276 Albian sandstones spanning the range of Site 398–Leg 149 values.

The overall higher potassium feldspar content of the Iberian sandstones (all ages) and low feldspar content of the Newfoundland margin samples can be linked to fundamental differences in geology across the Newfoundland–Iberia transect arising from the localization of rifting along a continental suture zone, the Hercynian Front (Fig. **F17**). To the west are the rocks of the Avalon Zone, discussed above, and to the east are a series of Variscan basement units (Fig. **F17**). Variscan metamorphic/plutonic basement produces feldspathic sand, as seen in the Leg 103 sandstones (Johnson, 1988; Winterer et al., 1988) and Cenozoic sandstones of Leg 149 (Marsaglia et al., 1996). Marsaglia et al. (1996) proposed that the likely source of sand at Leg 149 sites during the Cenozoic

F17. Tectonic terrane map of Grand Banks and Iberian regions, p. 32.

was the Rio Duero system, which drains Hercynian granites and metamorphic rocks. This hypothesis is borne out by the similarity of sand from within the Rio Duero and along the coast (Romeo, 2003) to Cenozoic sand recovered during Leg 149. The modern Tajo River to the south also drains Hercynian granites and metasedimentary basement rocks, producing feldspatholithic sand (average $Qm_{57}F_{35}Lt_8$ in lower reaches) with potassium feldspar more common than plagioclase feldspar (Le Pera and Arribas, 2004). In contrast, the headwaters of the river drain the Iberian range sourced by Neogene clastics derived from the Alpine orogen. Not surprisingly, the average composition of sand from the headwaters ($Qm_{67}F_4Lt_{29}$) is more similar to the Newfoundland samples. And indeed, the latter could also have been derived from foreland basin sediments produced during the Hercynian orogen. Recycling of Variscan–Hercyniaan sediments into the Site 1276 section is supported by **Wilson and Hiscott** (this volume), who found dominantly Variscan–Hercynian (270–320 Ma) white mica clasts in three samples from the bases of a middle Albian, a Turonian, and a middle Eocene turbidite bed. They suggest several possible sources of micas: (1) Iberian Variscan–Hercynian basement to the east, (2) Carboniferous igneous rocks from Newfoundland or Grand Banks, or (3) recycling of mica clasts derived from Iberia in older Mesozoic and/or upper Paleozoic sediments deposited in the Grand Banks area.

PALEOCENE VOLCANIC SAND PROVENANCE

Extension-related volcanism is thought to have ceased along the Newfoundland margin at the end of the Early Cretaceous (Grant and McAlpine, 1990), with the youngest igneous rocks recovered from the shelf (96.4 Ma; exploration well) and Newfoundland Seamounts (97.7 Ma; dredge) as summarized in Pe-Piper et al. (1990). Younger volcanic rocks (~59 Ma) are limited to rift zones to the north, east, and west of Greenland (Pe-Piper et al., 1990).

One of the more interesting sedimentological discoveries of Leg 210 was the isolated volcanic input at ~60 Ma in Core 210-1276A-15R, near the Unit 2/3 boundary. Shipboard petrographic observations showed this interval to contain felsic(?) and mafic epiclastic volcanic debris. The timing of this input at Site 1276, as verified by mica ages of ~57 Ma by **Wilson and Hiscott** (this volume), corresponds to a major uplift event followed by extensive magmatism and rifting off southeastern Greenland (e.g., Larson and Saunders, 1998). As documented at Site 917, the Greenland volcanism was bimodal with dacitic and basaltic end-members, and this bimodal episode was relatively short lived (61–60 Ma). It is possible that an event of this magnitude could have produced a submarine sediment pulse (fan) that crossed the Mid-Atlantic Ridge via a major transform zone and extended 1000 km south to the vicinity of Site 1276. Alternatively, the volcanic debris may have been derived from the little-studied Cretaceous Newfoundland Seamounts (Pe-Piper et al., 1990) located south of Site 1276 or perhaps some as-yet undocumented source on Grand Banks. In support of a seamount source, Davis et al. (2002) have shown through submersible sampling and mapping of seamount systems off the Pacific coast of North America that seamount reactivation may occur during regional tectonic reorganizations. In some cases during this rejuvenation phase, the seamounts can build to sea level and produce epiclastic debris like that observed in Core 210-1276A-15R.

Although several samples from Core 210-1276A-15R were collected for this study, they contained little to no volcaniclastic material. Two samples were point counted (Table T1), with LmlvLs%Lv ranging from 0.0% to 6.9%. However, significant (LmLvLs%Lv > 5%) volcanic contributions to the section were first noted in the Santonian samples and continue into the Eocene, suggesting that the few percent volcanic debris could be a background signal. It should be noted that Sample 210-1276A-15R-4, 123 cm, contained the highest percentage of mica (11%) in the Site 1276 section, and ages provided by **Wilson and Hiscott** (this volume) are consistent with a coeval volcanic source. However, geochemical studies of mudstones across this interval show no evidence of volcanic input (**Robertson,** this volume). The lack of tuffaceous fines suggests that the source of the bed described shipboard was different from the source providing fine background sediments. Questions remain as to the source(s) and modes of supply of volcanic material to this margin, as well as its Iberian conjugate, where volcaniclastics are also present, as shown below.

A review of the thin sections prepared from the ~60-Ma interval recovered on the Iberian margin shows them to contain heretofore unrecognized mafic to felsic(?) volcanic detritus: Samples 149-897C-62R-1, 123 cm (Fig. F18), 173-1068A-7R-2, 82 cm (Fig. F19), and 173-1069A-7R-2, 82 cm (Fig. F20). Their composition is masked by extreme alteration of glass to clay minerals; however, the common occurrence of black tachylitic microlitic fragments is consistent with a mafic source, and the presence of highly vesiculated pumice suggests a felsic component as well (Fig. F20). As with Site 1276, some of the debris is rounded and interpreted as epiclastic. This debris could have been derived from reactivated volcanic centers in the Lusitania Basin or perhaps on the Tore Seamount that lies along trend with the Newfoundland Seamounts (Fig. F4). These observations suggest the volcanic reactivation or exotic influx of volcanic material was not limited to the Newfoundland margin and was a punctuated (~60 Ma) but widespread event across the North Atlantic region.

PROVENANCE OF EOCENE SANDSTONES

Eocene clastic rocks at Site 1276 are truly grainstones or calcarenites with minor terrigenous components. They likely represent a continuum of mixing between two sources, one siliciclastic the other calcareous. As outlined above, the proportions and types of silicilastic grains in these sediments suggest a similar siliciclastic source to that of the underlying Cretaceous section. Additional evidence comes from the distribution of mica ages, which are also similar to Cretaceous samples (**Wilson and Hiscott,** this volume). The calcareous source was likely a carbonate shelf environment in that anomalous, large Eocene benthic foraminifers concentrated in Cores 210-1276A-7R through 15R are generally associated with warmer shallow-water reef environments (see discussion in Georgescu et al., submitted [N2]). Eocene grainstones are also present on the Iberian conjugate margin, but unlike the Site 1276 Eocene grainstones, the Site 398 samples contain mostly planktonic foraminifer bioclasts associated with recycled(?) carbonate lithic clasts that are present throughout the section (Table T1). The carbonate system on Galicia Bank likely extended to the Iberian shelf, in that Eocene sandstones recovered to the south (Fig. F4) during Legs 149 (Marsaglia et al., 1996) and 173 (Wallrabe-Adams, 2001) are also calcareous. Eocene fore-

F18. Photomicrographs of Sample 149-897C-62R-1, 123 cm, p. 33.

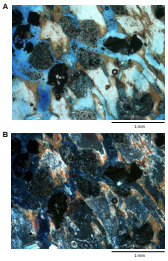

F19. Photomicrographs of Sample 173-1068A-7R-2, 82 cm, p. 34.

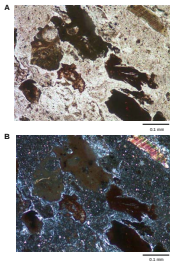

F20. Photomicrographs of Sample 173-1069A-7R-2, 82 cm, p. 35.

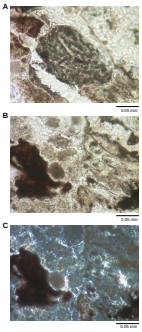

land basin clastic rocks of the Pyrenees are also similarly calcareous (Fontana et al., 1989), suggesting that this was a regional phenomenon. Because Fontana et al. (1989) worked with coarser arenites and microrudites, they were able to differentiate coeval intrabasinal intraclasts from detrital carbonate clasts supplied by upthrusted Cretaceous carbonate units. In contrast, bioclastic debris is the main indicator of recycling within the fine to very fine sandstones at Site 1276 (Georgescu et al., submitted [N2]). Fontana et al. (1989) report large quantities of intrabasinal bioclastic debris such as benthic and planktonic foraminifers, bryozoans, echinoderms, algal grains, and shell fragments. Despite the active tectonic setting of the Pyrenees during the Eocene, Fontana et al. (1989) called on eustacy to explain the carbonate-rich sandstones, through intrabasinal carbonate input during sea level rise and erosion of highstand carbonate complexes during sea level fall. Similar eustatic-driven processes may have been acting along the Newfoundland margin during the Eocene, but in a passive margin rather than a foreland basin setting.

MODELS OF RIFT-TO-DRIFT EVOLUTION

Leg 210, in conjunction with ODP Legs 149 and 173 and DSDP Site 398, was conceptualized as the first test of directly conjugate margins, with the goal of documenting basin architecture and evolution from rift-to-drift stages. Although only part of the drift history is represented by the sections successfully cored during Leg 210, this stratigraphy can be directly compared to that cored on the Iberian margin. Previously collected petrologic data sets from petroleum exploration wells on the Newfoundland margin and Iberian Legs 103 (Johnson, 1988) and 149 (Marsaglia et al., 1996) were combined with data collected in this study (Sites 1276, 398, 1065, and 1069) to compare the records of coarse clastic sedimentation on these margins and to synthesize a general model for rift-to-drift evolution as described below.

Petrofacies models for rift-to-drift successions along continental margins have not been adequately defined in the literature in part because these thick sedimentary successions often limit availability of the early rift facies (Marsaglia, 1991). Thus, the Iberian/Newfoundland conjugate pair was chosen because of their thin sedimentary cover as compared to other passive margins, such as the northern Gulf of Mexico. In a study of modern Rio Grande Rift sand petrofacies, Ingersoll (1990) showed that synrift petrofacies can be quite variable, depending on the distribution of prerift basement and sedimentary cover, as well as the distribution of synrift volcanic centers (Fig. F21). Garzanti et al. (2001) followed with an actualistic study of proto-oceanic basins, the Red Sea and Gulf of Aden, where there are distinct changes associated with the distribution and amount of synrift volcanism and degree of unroofing of crystalline basement. The undissected rift shoulders shed quartzose sand recycled from cratonic cover sequences, which when progressively removed expose basement terrains that yield quartzofeldspathic sand (Fig. F21). The margins characterized by volcanism first yield volcaniclastic successions, then when erosion is sufficient to remove the volcanic cover, they yield quartzofeldspathic basement-derived sand. Thus both volcanic and nonvolcanic rifted margins converge to basement-derived sand compositions in this young system. The geological record of Red Sea rifting is defined in the Gulf of Suez, where uplift associated with continental rifting results in the unroofing of crystalline basement

F21. QFL plots of rift and young ocean basin sand compositions, p. 36.

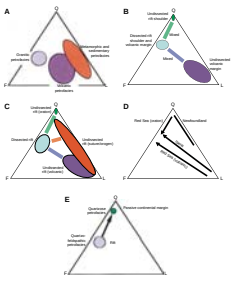

rocks (Steckler and Omar, 1994). Petrologic evidence for this unroofing is recorded in the synrift sedimentary pile of the Gulf of Suez where clast populations show an inverted stratigraphy: clasts of younger formations in the oldest synrift section and older formations, including crystalline basement, in the younger synrift formations (Evans, 1990). Arribas et al. (2003) describe the fluvio-lacustrine fill of an intraplate rift basin in north central Spain and relate associated quartzose sand petrofacies to basement geology, paleogeography, and basin evolution. The range of compositions encountered in the synrift fill of the basin reflect local metamorphic, plutonic, and recycled sedimentary source rocks.

In his classic synthesis, Dickinson (1985) somewhat ignored rifted and passive margin settings but inferred that during the rift-to-drift transition in passive margin successions, sand would be first quartzofeldspathic (basement uplift during rifting) then more quartzose (reworking and larger river systems) upsection (Fig. F21). This model does not hold for the Iberian–Newfoundland system. On the Iberian margin there is a progression from lithic sandstones to more quartzofeldspathic sandstones that Marsaglia et al. (1996) attributed to unroofing or development of the fluvial systems that fed submarine fans. Prerift and rift data from Galicia Bank to the north (Johnson, 1988) also show the production of lithic-rich sandstones during rifting (Fig. F22), but quartzofeldspathic prerift sandstones suggest that basement terrains were already exposed, perhaps during an earlier rift phase. Lithic fragments in these examples were mainly sedimentary and metamorphic debris.

As stated earlier, synrift sandstones were not recovered at Site 1276, but the fill of the older Jeanne d'Arc rift basin and the postrift sections at Site 1276 suggest that this margin is characterized by more quartzolithic sandstones, both in the synrift and postrift rift units (Fig. F22). This may be a product of the fundamental differences between Iberian and Newfoundland Paleozoic geology. The Newfoundland sand compositions fall in the recycled orogen field of Dickinson (1985) and are consistent with having been recycled from older foreland basins sediments shed westward off the Hercynian orogen, whose dissected batholithic roots to the east, unroofed by rifting, now supply quartzofeldspathic sand to the Iberian passive margin.

Thus rift-to-drift transitions may have several evolutionary pathways depending on the importance of synrift volcanism and the nature of the continental successions (basement and cover sequences) within the rifted segment (Fig. F21). Lithic-rich synrift sandstones are the norm, except where the cover sequences are semiconsolidated quartzose sandstones. In that case, the recycled sediments are themselves quartzose (see also Arribas et al., 2003). If crystalline basement is minimally present or not exposed during rift or drift phases, such as in the case of the Newfoundland margin, then synrift and postrift sandstones may have very similar quartzolithic compositions (Fig. F21).

F22. Paleogeographic reconstructions of Newfoundland–Iberian conjugate margins, p. 37.

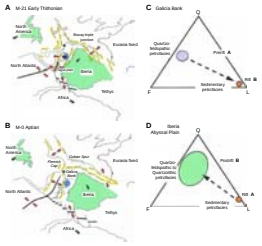

CONCLUSIONS

Detrital modes of Albian and younger Cretaceous sandstones at Site 1276 are similar and suggest that there was one major source of sandy sediment. Because this site was within a narrow ocean basin at this time, an eastern Iberian source was considered. The few Albian data available from the Iberian margin are inconclusive, but when Mesozoic–Cenozoic detrital modes for both margins are considered as a whole, the Site 1276 detrital modes are more compatible with a New-

foundland margin source such as Avalon Uplift. Other studies (e.g., Hiscott, this volume) help to rule out more northerly sources such as the lesser known rocks of Flemish Cap. The Site 1276 sandstones have a recycled orogen (Dickinson, 1985) provenance, consistent with their being at least partly derived from the erosion and recycling of foreland basin sedimentary cover sequences.

The source(s) of the ~60-Ma volcanic debris at Site 1276 remains unknown. Although we found no additional volcanic-rich intervals in samples from this core, we did identify and document mafic to felsic debris from the ~60-Ma intervals at several sites drilled on the Iberian transect. This new information implies that magmatism was widespread across the North Atlantic during this time frame. The presence of volcaniclastic material off Iberia makes long-distance submarine transport from Greenland volcanic centers less feasible; we favor local basin margin or intrabasinal sources (reactivation?) with eruptions likely linked to rifting and plate reorganizations in the North Atlantic.

The upsection change to a more calcareous petrofacies (grainstones) was likely driven by the establishment of carbonate environments on Grand Banks. This appears to have been a regional North Atlantic phenomenon, with calcareous deposits characterizing both the western and eastern (Pyrenees) margins of the Iberian Peninsula as well. Shelf productivity and downslope distribution of calcareous debris was likely eustatically controlled.

The Newfoundland and Iberian margin rift-to-drift successions and associated petrofacies are part of a spectrum summarized in Figure F21. The nonparallel compositional evolution of these margins is linked to the asymmetry of basement terranes across the region associated with rifting along a former suture zone. The more mature sand compositions likely result from reworking of foreland basin sediments. This asymmetry may be present elsewhere along the margins of the Atlantic Ocean. As sand composition exerts a first-order control on diagenesis and ultimate sandstone reservoir character on passive margins, this model has important ramifications in petroleum exploration.

ACKNOWLEDGMENTS

This research used samples and data provided by the Ocean Drilling Program (ODP). ODP is sponsored by the U.S. National Science Foundation (NSF) and participating countries under management of Joint Oceanographic Institutions (JOI), Inc. Funding for this study was provided to Marsaglia by JOI. We thank Emilia Le Pera and José Arribas for their reviews.

REFERENCES

Arribas, J., Alonso, A., Mas, R., Tortosa, A., Rodas, M., Barrenechea, J.F., Alonso-Azcárate, and Artigas, R., 2003. Sandstone petrography of continental depositional sequences of an intraplate rift basin: western Cameros Basin (north Spain). *J. Sediment. Res.,* 73(2):309–327.

Bell, J.S., and Howie, R.D., 1990. Paleozoic geology. *In* Keen, M.J., and Williams, G.L. (Eds.), *Geology of the Continental Margin of Eastern Canada*. Geol. Soc. Am., 2:141–165.

Boillot, G., Mougenot, D., Girardeau, J., and Winterer, E.L., 1989. Rifting processes of the West Galicia margin, Spain. *In* Tankard, A.J., and Balkwill, H.R. (Ed.), *Extensional Tectonics and Stratigraphy of the North Atlantic Margins*. AAPG Mem., 46:363–377.

Brown, D.M., McAlpine, K.D., and Yole, R.W., 1989. Sedimentology and sandstone diagenesis of Hibernia formation in Hibernia oil field, Grand Banks of Newfoundland. *AAPG Bull.,* 73(5):557–575.

Capdevila, R., and Mougenot, D., 1988. Pre-Mesozoic basement of the western Iberian continental margin and its place in the Variscan Belt. *In* Boillot, G., Winterer, E.L., et al., *Proc. ODP, Sci. Results,* 103: College Station, TX (Ocean Drilling Program), 3–12. **doi:10.2973/odp.proc.sr.103.116.1988**

Carozzi, A.V., 1989. *Carbonate Rock Depositional Models: A Microfacies Approach:* Englewood Cliffs, NJ (Prentice Hall).

Davis, A.S., Clague, D.A., Bohrson, W.A., Dalrymple, G.B., and Greene, H.G., 2002. Seamounts at the continental margin of California: a different kind of oceanic intraplate volcanism. *Geol. Soc. Am. Bull.,* 114:316–333. **doi:10.1130/0016-7606(2002)114<0316:SATCMO>2.0.CO;2**

Dickinson, W.R., 1985. Interpreting provenance relations from detrital modes of sandstones. *In* Zuffa, G.G. (Ed.), *Provenance of Arenites:* Dordrecht (D. Riedel), 333–361.

Evans, A.L., 1990. Miocene sandstone provenance relations in the Gulf of Suez: insights into synrift unroofing and uplift history. *AAPG Bull.,* 74:1386–1400.

Fontana, D., Zuffa, G.G., and Garzanti, E., 1989. The interaction of eustacy and tectonism from provenance studies of the Eocene Hecho group turbidite complex (south-central Pyrenees, Spain). *Basin Res.,* 2:223–237.

Garzanti, E., Vezzoli, G., Andò, S., and Castiglioni, G., 2001. Petrology of rifted-margin sand (Red Sea and Gulf of Aden, Yemen), *J. Geol.,* 109(3):277–297. **doi:10.1086/319973**

Grant, A.C., and McAlpine, K.D., 1990. The continental margin around Newfoundland. *In* Keen, M.J., and Williams, G.L. (Eds.), *Geology of the Continental Margin of Eastern Canada*. Geol. Surv. Can., Geol. of Can., 2:239–292.

Hesse, R., and Abid, I.A., 1998. Carbonate cementation—the key to reservoir properties of four sandstone levels (Cretaceous) in the Hibernia oil field, Jeanne d'Arc Basin, Newfoundland, Canada. *In* Morad, S. (Ed.), *Carbonate Cementation in Sandstones*. Spec. Publ. Int. Assoc. Sedimentol., 26:363–393.

Ingersoll, R.V., 1990. Actualistic sandstone petrofacies; discriminating modern and ancient source rocks. *Geology,* 18(8):733–736. **doi:10.1130/0091-7613(1990)018<0733:ASPDMA>2.3.CO;2**

Ingersoll, R.V., Bullard, T.F., Ford, R.L., Grimm, J.P., Pickle, J.D., and Sares, S.W., 1984. The effect of grain size on detrital modes: a test of the Gazzi-Dickinson point-counting method. *J. Sediment. Petrol.,* 54:103–116.

Jansa, L.F., and Wade, J.A., 1975. Geology of the continental margin off Nova Scotia and Newfoundland. *In* Linden, W.J.M., and Wade, J.A. (Eds.), *Offshore Geology of Eastern Canada* (Vol. 2): *Regional Geology.* Pap.—Geol. Surv. Can., 51–105.

Johnson, J.A., 1988. Composition of Lower Cretaceous sandstone, Galicia margin. *In* Boillot, G., Winterer, E.L., et al., *Proc. ODP, Sci. Results,* 103: College Station, TX (Ocean Drilling Program), 505–512. **doi:10.2973/odp.proc.sr.103.127.1988**

Kairo, S., Suttner, L.J., and Dutta, P.K., 1993. Variability in sandstone composition as a function of depositional environment in coarse-grained delta system. *In* Johns-

son, M.J., and Basu, A. (Eds.), *Processes Controlling the Composition of Clastic Sediments:* Spec. Pap.—Geol. Soc. Am., 284:41–65.

Larson, H.C., and Saunders, A.D., 1998. Tectonism and volcanism at the southeast Greenland rifted margin: a record of plume impact and later continental rupture. *In* Saunders, A.D., Larson, H.C., and Wise, S.W., Jr. (Eds.), *Proc. ODP, Sci. Results,*152: College Station, TX (Ocean Drilling Program), 503–533. **doi:10.2973/odp.proc.sr.152.240.1998**

Le Pera, E., and Arribas, J., 2004. Sand composition in an Iberian passive-margin fluvial course: the Tajo River. *Sediment. Geol.,* 171:261–281. **doi:10.1016/j.sedgeo.2004.05.019**

Marsaglia, K.M., 1991. Provenance of sands and sandstones from a rifted continental arc, Gulf of California, Mexico. *In* Fisher, R.V., and Smith, G.A. (Eds.), *Sedimentation in Volcanic Settings.* Spec. Publ.—SEPM (Soc. Sediment. Geol.), 45:237–248.

Marsaglia, K.M., García y Barragán, J.C., Padilla, I., and Milliken, K.L., 1996. Evolution of the Iberian passive margin as reflected in sand provenance. *In* Whitmarsh, R.B., Sawyer, D.S., Klaus, A., and Masson, D.G. (Eds.), *Proc. ODP, Sci. Results,* 149: College Station, TX (Ocean Drilling Program), 269–280. **doi:10.2973/odp.proc.sr.149.201.1996**

Marsaglia, K.M., and Tazaki, K., 1992. Diagenetic trends in Leg 126 sandstones. *In* Taylor, B., Fujioka, K., et al., *Proc. ODP, Sci. Results,* 126: College Station, TX (Ocean Drilling Program), 125–138. **doi:10.2973/odp.proc.sr.126.123.1992**

Pe-Piper, G., Piper, D.J.W., Keen, M.J., and McMillan, N.J., 1990. Igneous rocks of the continental margin: tectonic and geophysical overview. *In* Keen, M.J., and Williams, G.L. (Eds.), *Geology of the Continental Margin of Eastern Canada*. Mem.—Geol. Soc. Am., 2:855.

Romeo, S., 2003. Studio composizionale della sabbie costiere e fluviale del tratto compreso tra la foce del fiume Duero e la voce del fiume Tajo, Portogallo [M.S. thesis]. Universita degli Studi della Calabria, Tesi di Laurea.

Shipboard Scientific Party, 1979. Site 398. *In* Sibuet, J.-C., Ryan, W.B.F., et al., *Init. Repts. DSDP,* 47 (Pt. 2): Washington (U.S. Govt. Printing Office), 25–233.

Sibuet, J.-C., Ryan, W.B.F., et al., 1979. *Init. Repts. DSDP,* 47 (Pt. 2): Washington (U.S. Govt. Printing Office).

Steckler, M.S., and Omar, G.I., 1994. Controls on erosional retreat of the uplifted rift flanks at the Gulf of Suez and northern Red Sea. *J. Geophys. Res.,* 99(B6):12159–12173. **doi:10.1029/94JB00278**

Tucholke, B.E., Sibuet, J.-C., Klaus, A., et al., 2004. *Proc. ODP, Init. Repts.,* 210: College Station, TX (Ocean Drilling Program). **doi:10.2973/odp.proc.ir.210.2004**

Wallrabe-Adams, H.-J., 2001. Data report: lithology and microfacies of Late Cretaceous to early Tertiary turbidites from Sites 1068 and 1069. *In* Beslier, M.-O., Whitmarsh, R.B., Wallace, P.J., and Girardeau, J. (Eds.), *Proc. ODP, Sci. Results,* 173: College Station, TX (Ocean Drilling Program), 1–35. **doi:10.2973/odp.proc.sr.173.013.2001**

Winterer, E.L., Gee, J.S., and Van Waasbergen, R.J., 1988. The source area for Lower Cretaceous clastic sediments of the Galicia margin: geology and tectonic and erosional history. *In* Boillot, G., Winterer, E.L., et al., *Proc. ODP, Sci. Results,* 103: College Station, TX (Ocean Drilling Program), 697–732. **doi:10.2973/odp.proc.sr.103.181.1988**

Ziegler, P.A., 1989. Evolution of the North Atlantic—an overview. *In* Tankard, A.J., and Balkwill, H.R. (Eds.), *Extensional Tectonics and Stratigraphy of the North Atlantic Margins*. AAPG Mem., 46:111–129.

APPENDIX

Point-count categories are listed in Table AT1. The point-count data collected for this study are in Table AT2.

AT1. Point-count categories, p. 42.

AT2. Point-count data, p. 43.

Figure F1. Bathymetric map showing locations of Leg 210 sites and submarine features mentioned in the text. Smts. = seamounts.

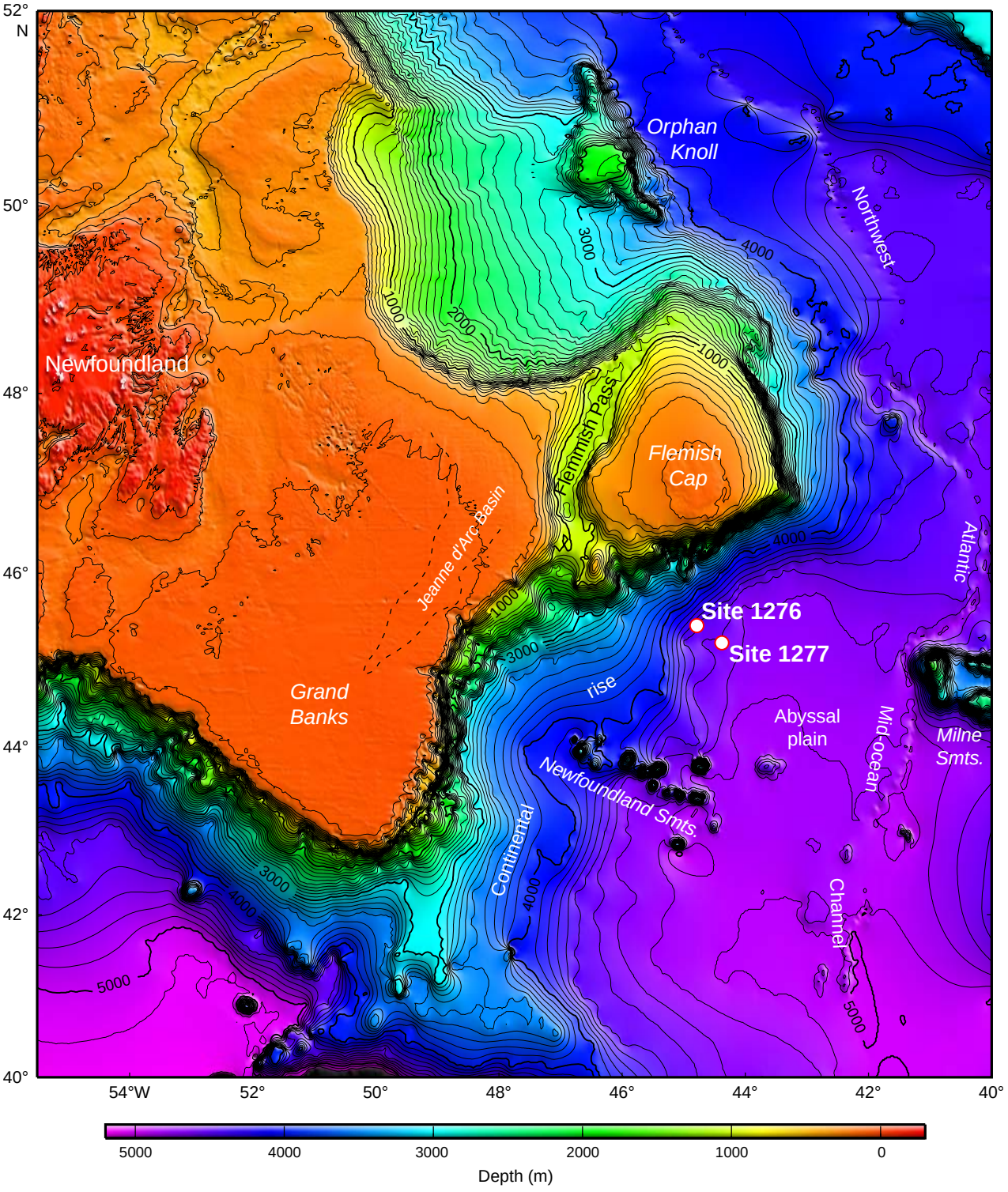

Figure F2. Summary stratigraphic column for Hole 1276A (modified from Tucholke, Sibuet, Klaus, et al., 2004). Core recovery is indicated by black rectangles in column on left. Triangles mark sampled intervals; symbols for point-counted sandy samples in this study are solid. TS = thin sections.

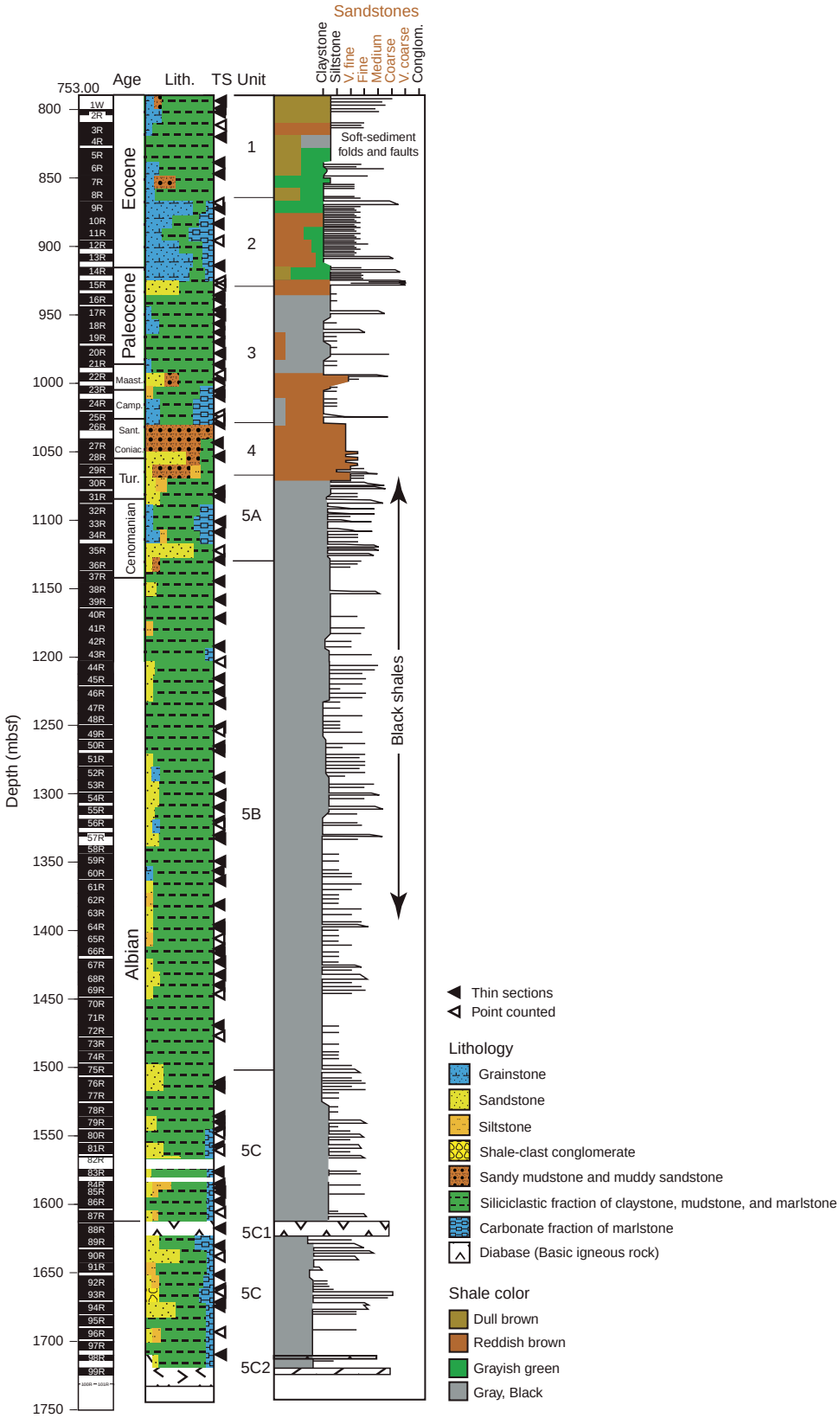

Figure F3. Stratigraphic column for DSDP Site 398 (after Sibuet, Ryan, et al., 1979, and Shipboard Scientific Party, 1979). Triangles mark sampled intervals; symbols for point-counted sandy samples are solid.

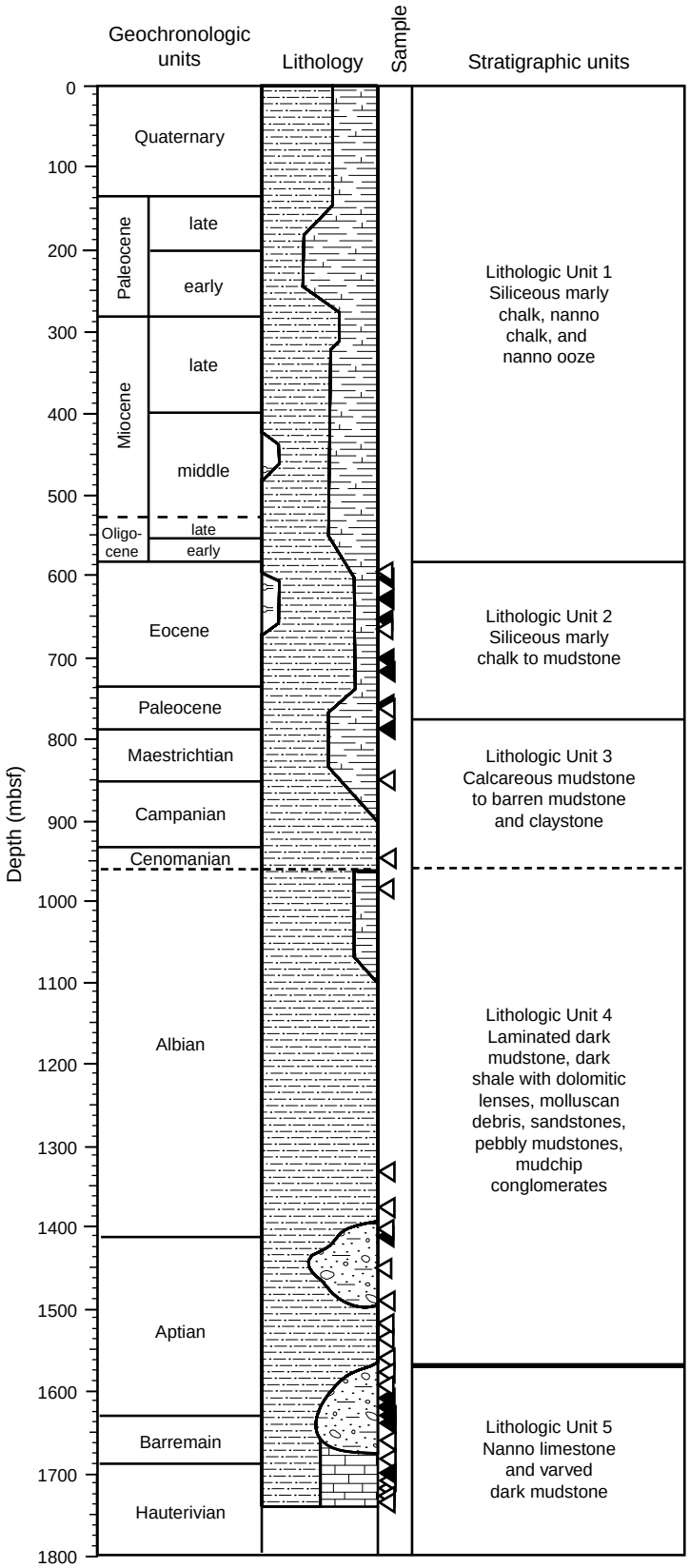

Figure F4. Reconstruction of the Newfoundland–Iberia conjugate margins at 121 Ma with locations of ODP Leg 210 Site 1276 in the Newfoundland Basin and DSDP and ODP sites on the Iberia margin highlighted in red. Blue = ocean crust, orange = evaporites in continental rift basins (modified from Tucholke, Sibuet, Klaus, et al., 2004). Bmt. = basement, Smt(s). = seamount(s), Nfld. = Newfoundland, A.P. = abyssal plain, Fl. = Flemish, N.B. = Newfoundland Basin, F.Z. = fracture zone, T.Z. = transition zone.

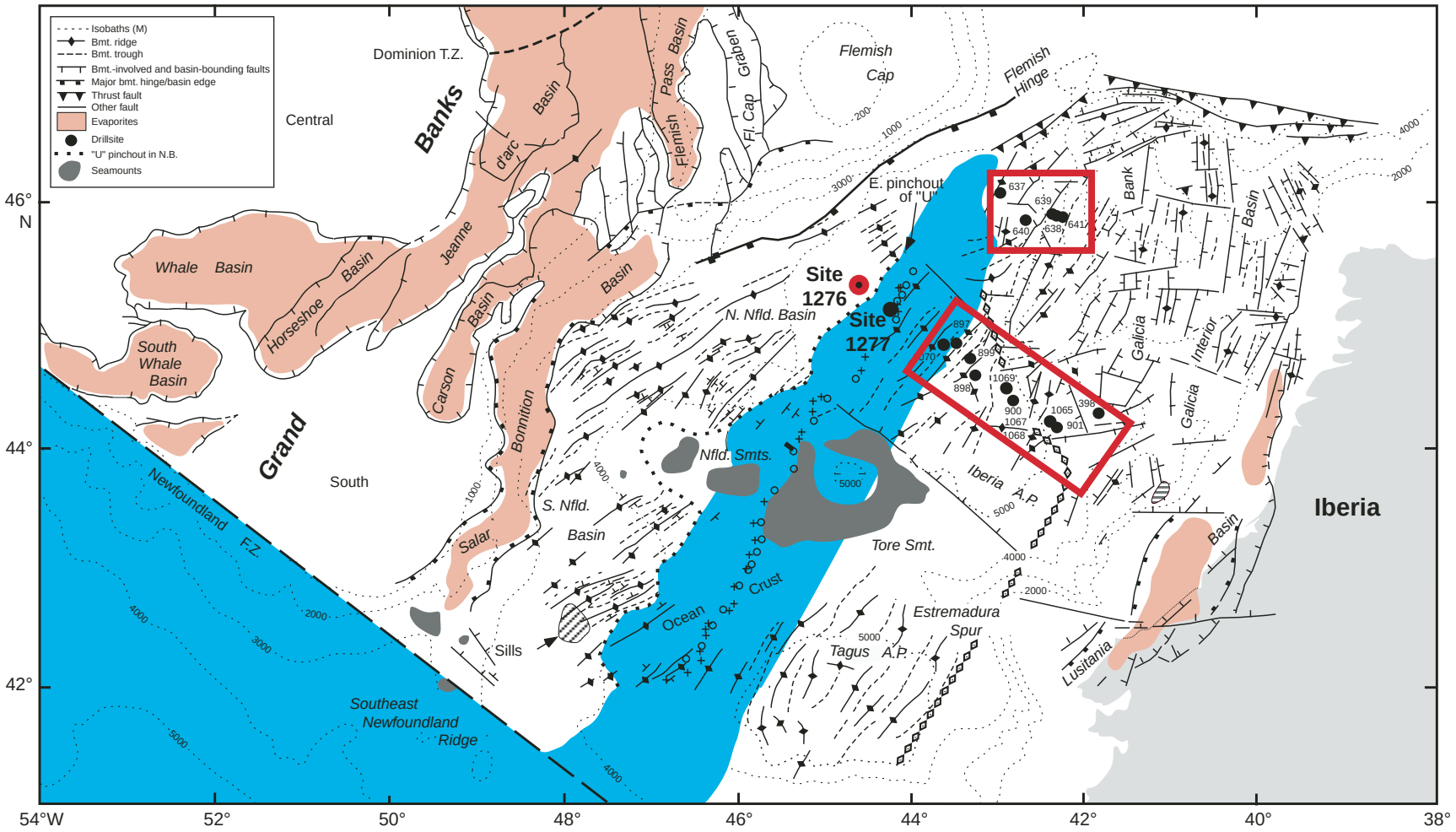

Figure F5. Blue epoxy-filled primary interparticle, primary intraparticle (within foraminifers), and secondary intraparticle (dissolution of siliceous sponge spicules) microporosity (Sample 210-1276A-9R-5, 118 cm). Area is a sandy burrow fill with a mixture of detrital grains including quartz, plagioclase, muscovite, glauconite, and coarse carbonate, as well as a variety of foraminifers. **A.** Plane-polarized light. **B.** Cross-polarized light.

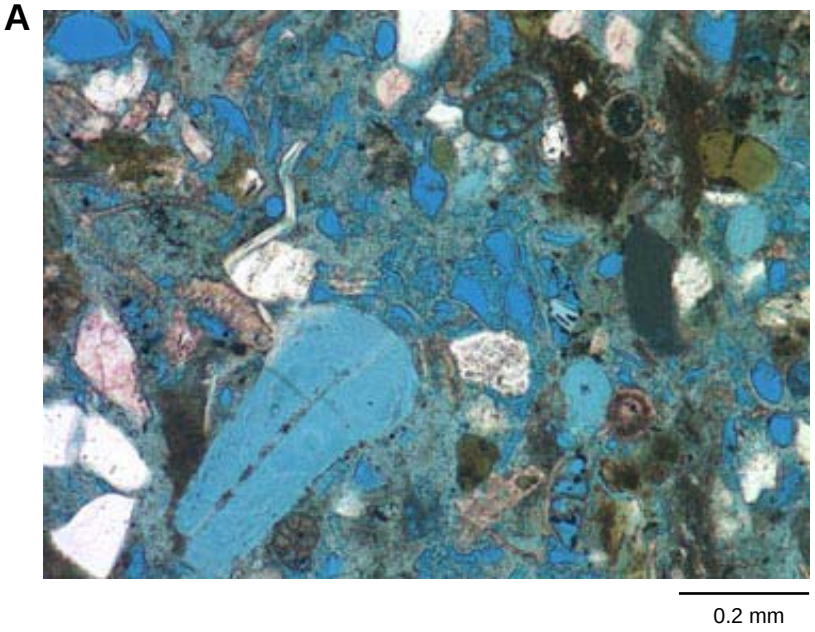

Figure F6. Typical Albian sandstone illustrating the effects of staining for feldspar recognition (Sample 210-1276A-49R-2, 130 cm). Grains outlined with dark golden yellow stain (also along cleavage) are potassium feldspar, pale pink grains are Ca-rich plagioclase feldspar, whereas more albitic grains are etched but not stained. **A.** Plane-polarized light. **B.** Cross-polarized light. Note the patchy birefringence exhibited by poikilotopic interparticle carbonate cement.

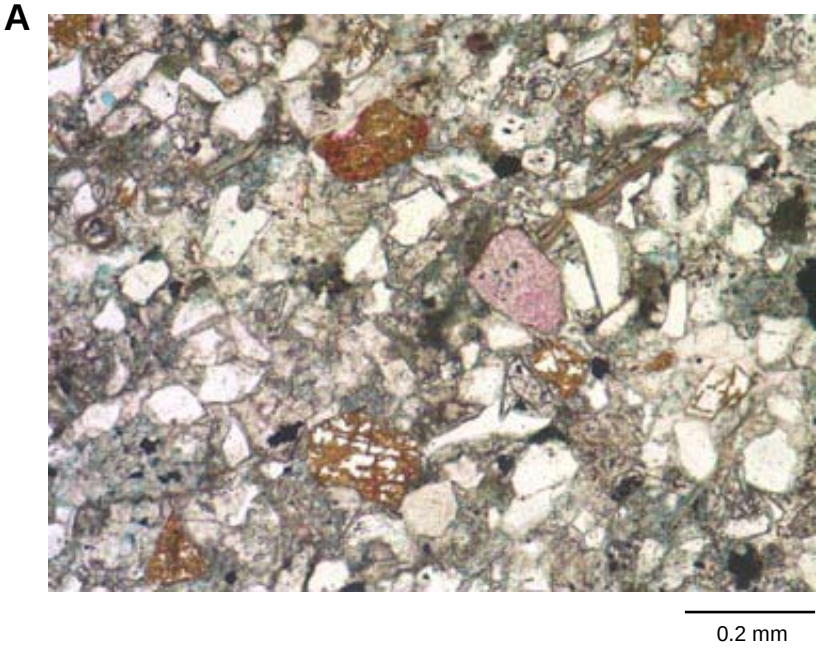

Figure F7. Metasedimentary rock fragments, altered biotite, muscovite/quartz intergrowth, and monocrystalline quartz set in a microcrystalline carbonate cement (Sample 210-1276A-81R-3, 134 cm). **A.** Plane-polarized light. **B.** Cross-polarized light.

Figure F8. Large metasedimentary rock fragment consisting of quartz and feldspar silt in a micaceous groundmass (Sample 210-1276A-93R-1, 24 cm). Note blue secondary pore in clast (dissolved feldspar or dense mineral?). **A.** Plane-polarized light. **B.** Cross-polarized light.

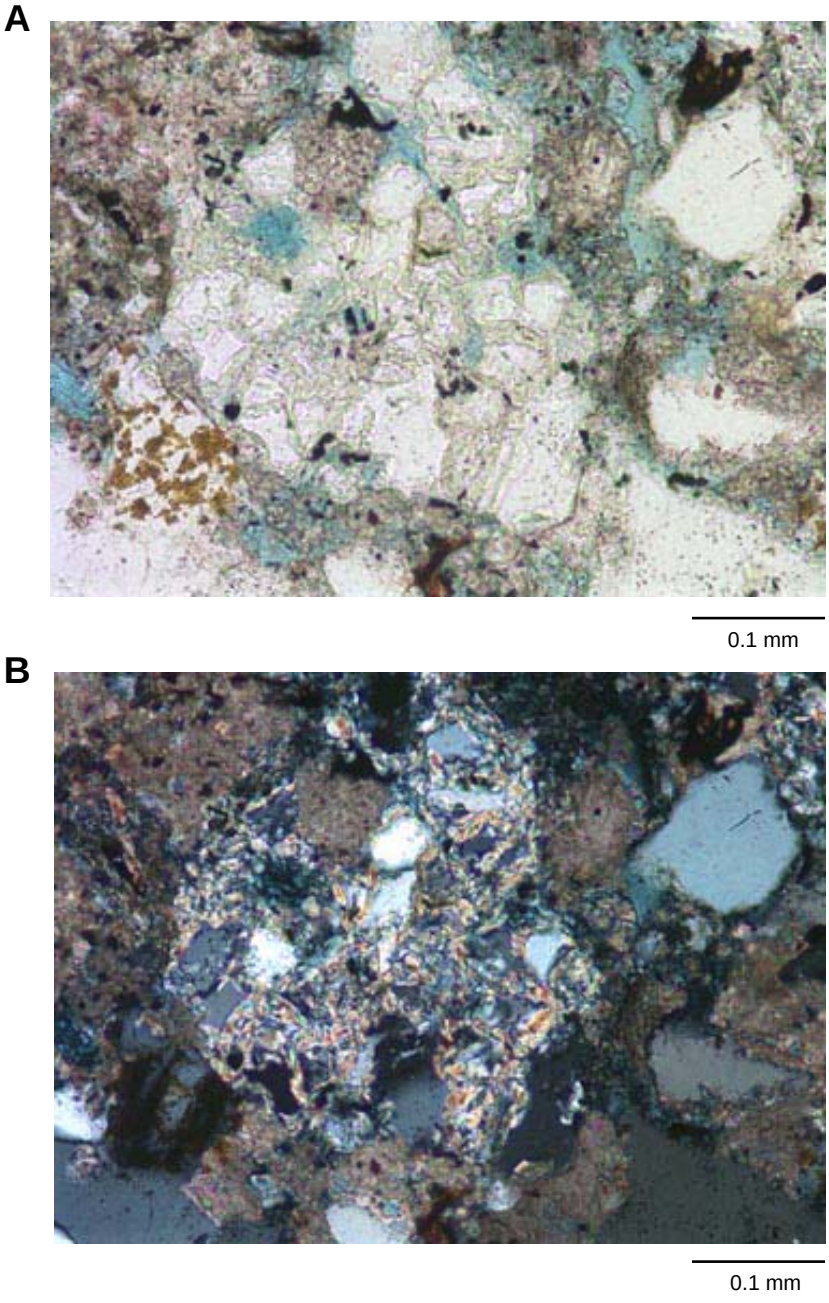

Figure F9. Mix of patchy carbonate and microporous (blue) kaolinite? (Sample 210-1276A-90R-5, 87 cm). Authigenic phases may be replacing feldspar grain. **A.** Plane-polarized light. **B.** Cross-polarized light.

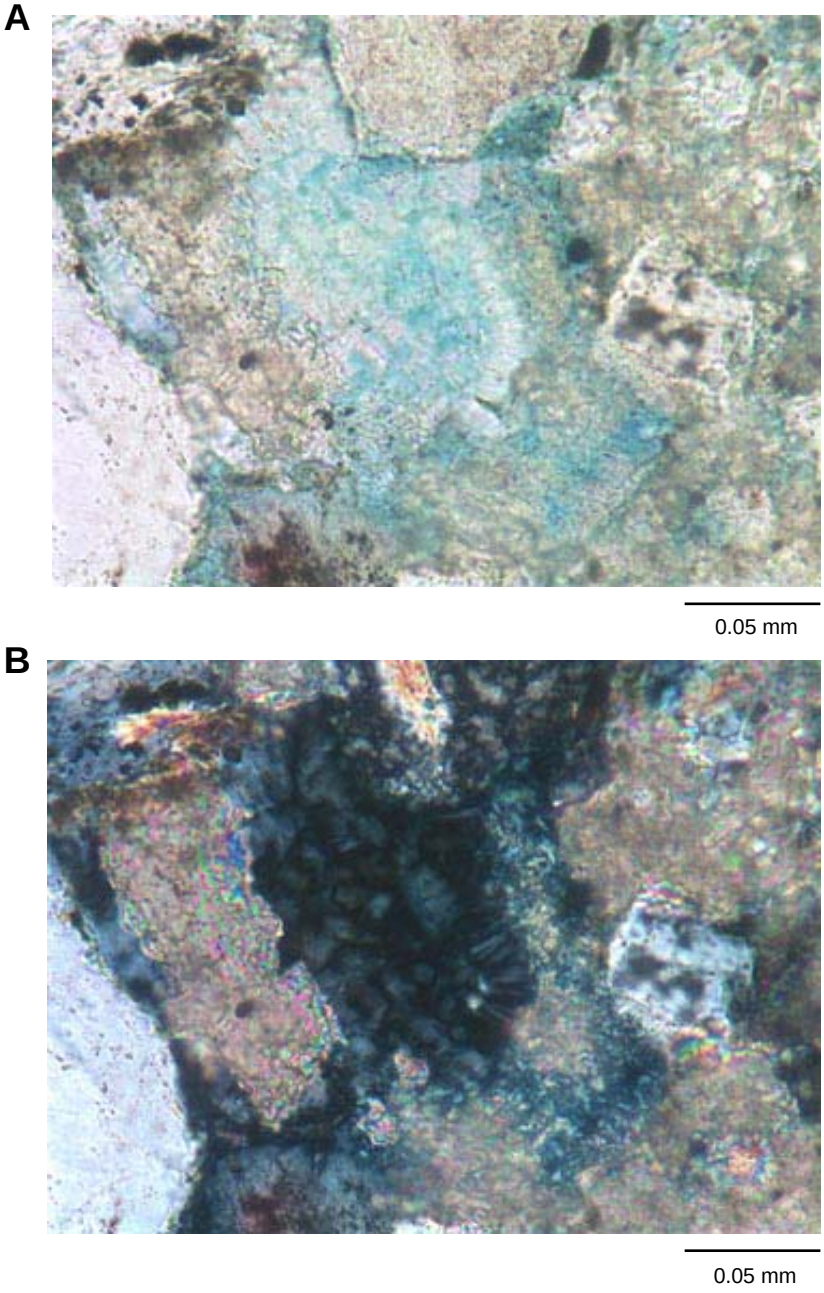

Figure F10. Ternary QFL plot of Albian and Aptian sandstone data from Grand Banks, ODP Site 1276, and Iberian ODP and DSDP sites. Data for Sites 1276 and 398 are presented in Table T1, p. 38. EC = two data points for samples of Early Cretaceous age from Marsaglia et al. (1996). Sources for other data as indicated. Note that L pole includes sedimentary carbonate lithic fragments. Symbols for Site 1276 samples are keyed on the plot according to sample ages.

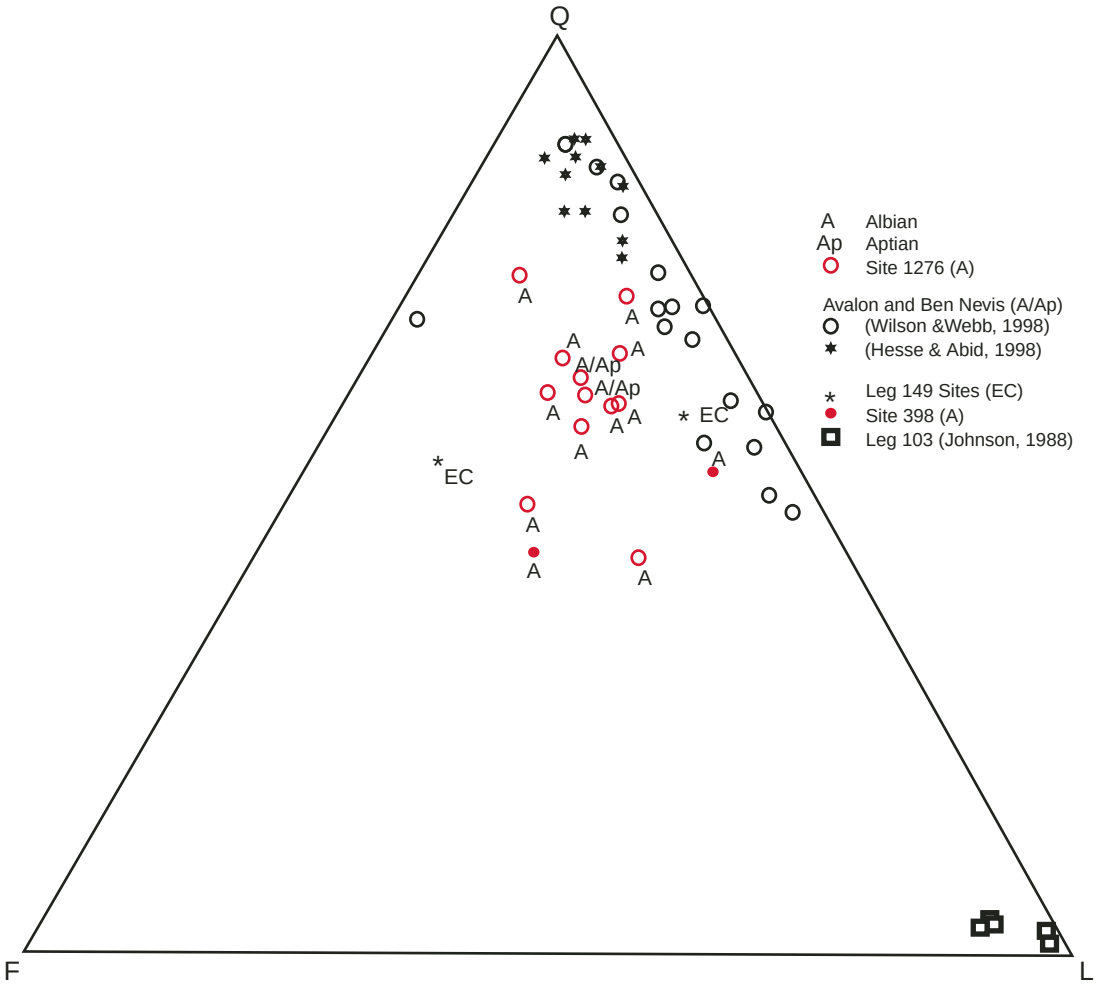

Figure F11. Ternary QFL plot of Cenomanian, Santonian, Campanian, and Maastrichtian sandstone data from ODP Site 1276 and Iberian ODP Site 1069. Data for Sites 1276 and 1069 are presented in Table T1, p. 38. Note that L pole includes sedimentary carbonate lithic fragments. Symbols for samples from Sites 1276 and 1069 are keyed on the plot according to sample ages.

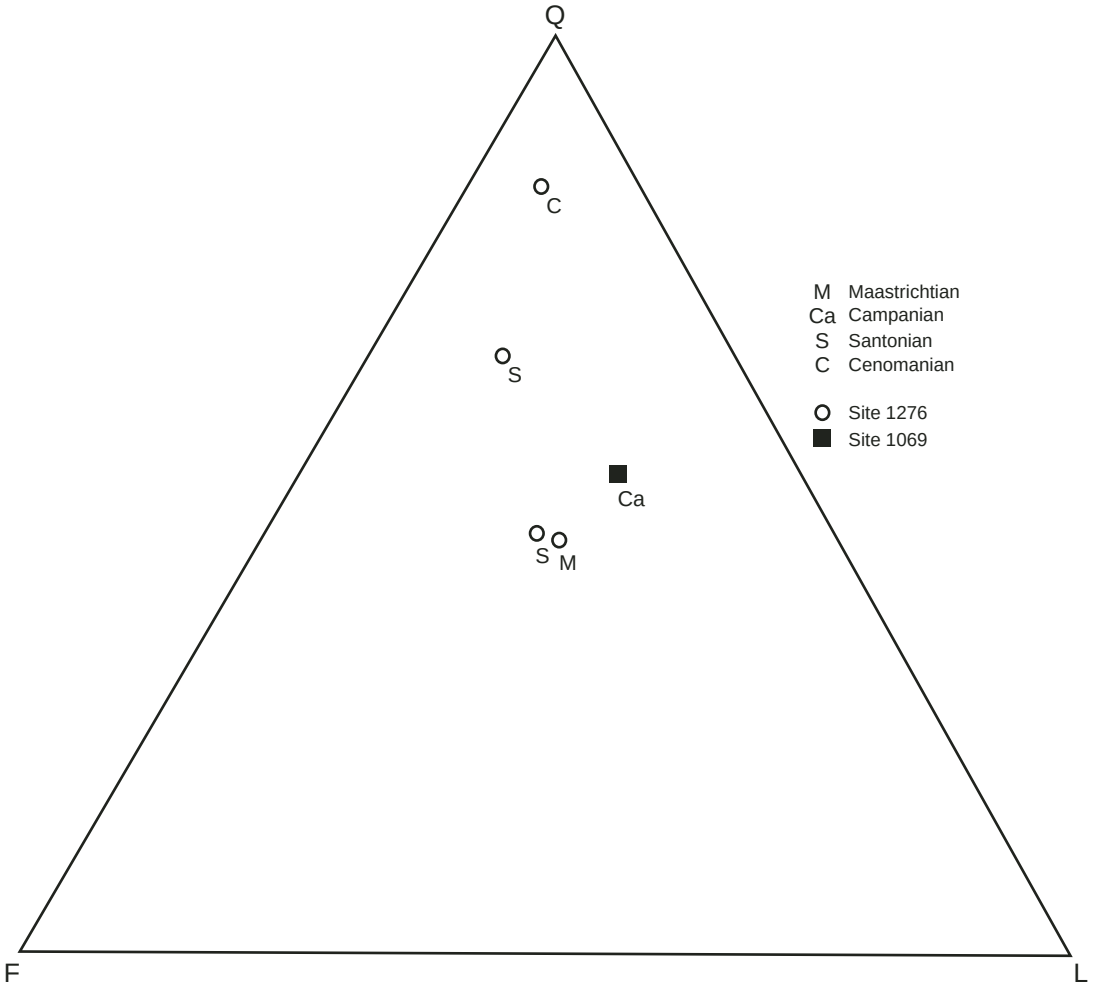

Figure F12. Ternary QFL plot of Eocene and Paleocene sandstone data from ODP Site 1276 and Iberian ODP and DSDP sites. Data for Sites 1276 and 398 are presented in Table T1, p. 38. Data for Leg 149 sites taken from Marsaglia et al. (1996). Polygon for middle Eocene is field of variation created by intersection of standard deviations about the mean. Note that L pole includes sedimentary carbonate lithic fragments. Symbols for samples are keyed on the plot according to sample ages.

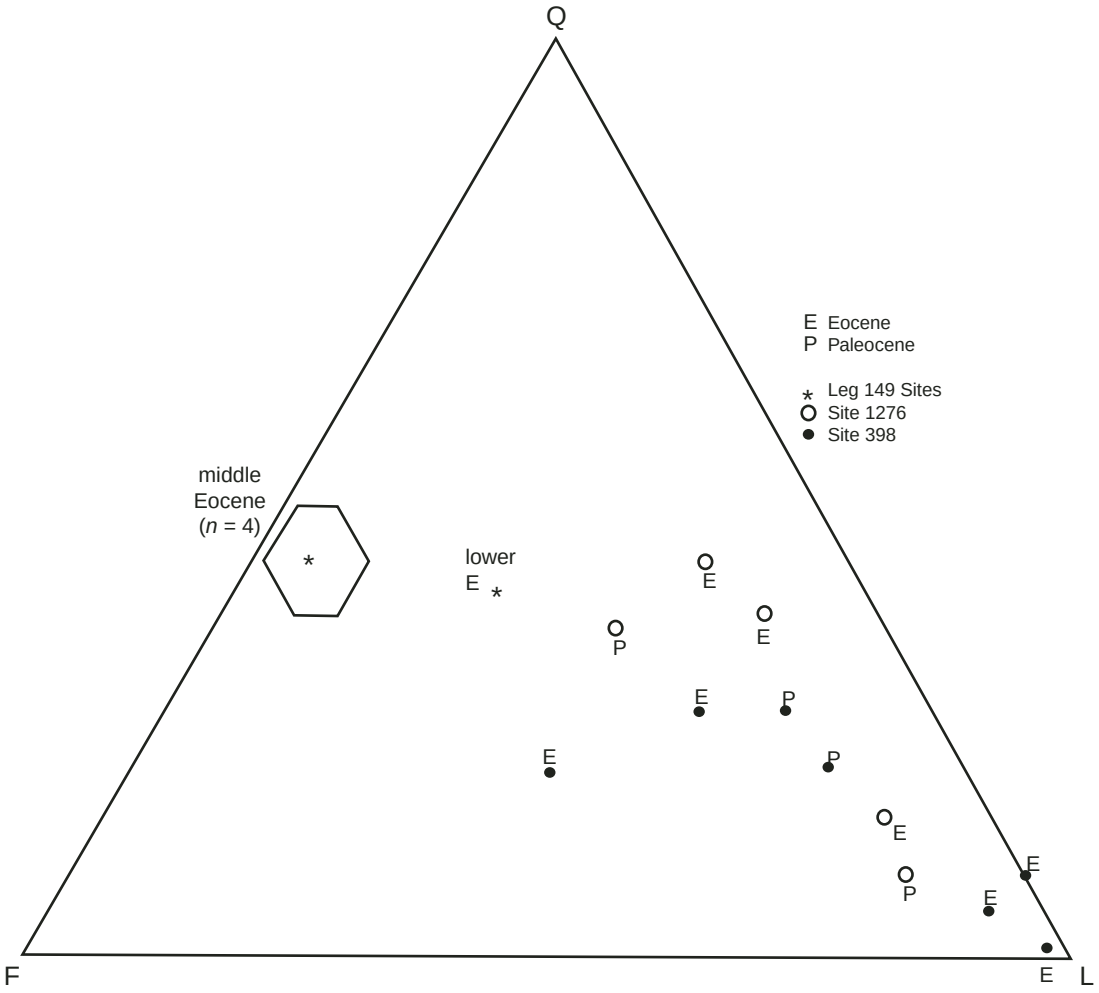

Figure F13. Histograms displaying the proportions of sedimentary lithic fragments (LmLvLs%Ls) for Site 1276, Leg 149 (Iberia), and Galicia Bank (Site 398 and Leg 103) sites. Data for Sites 1276 and 398 are presented in Table T1, p. 38. The Leg 149 data come from Marsaglia et al. (1996) and Leg 103 data from Johnson (1988).

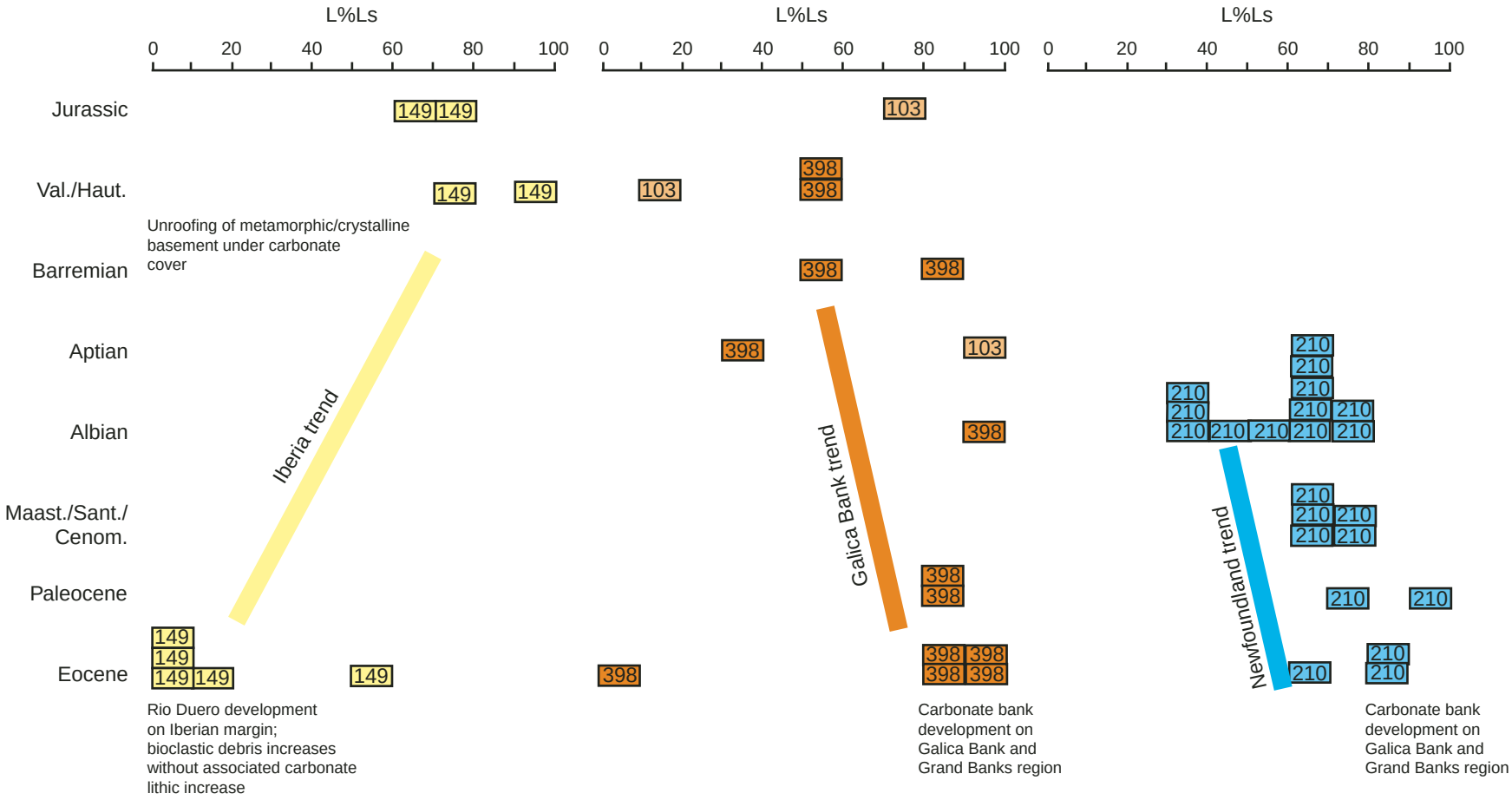

Figure F14. Ternary QmKP plot of Hauterivian–Eocene sandstone data from Grand Banks, ODP Site 1276, and Iberian ODP and DSDP sites. Data for Sites 1276 and 398 are presented in Table T1, p. 38. Data for Leg 149 sites taken from Marsaglia et al. (1996). Sources for other data as indicated. Only mean values for Galicia Bank (Leg 103) data shown to simplify diagram. Note range of K values more limited for Newfoundland (NF) margin samples and that Iberian/Galician samples are the most enriched in potassium feldspar. Symbols for samples are keyed on the plot according to sample ages. Valan = Valanginian, Tith = Tithonian. Polygon is field of variation created by intersection of standard deviations about the mean.

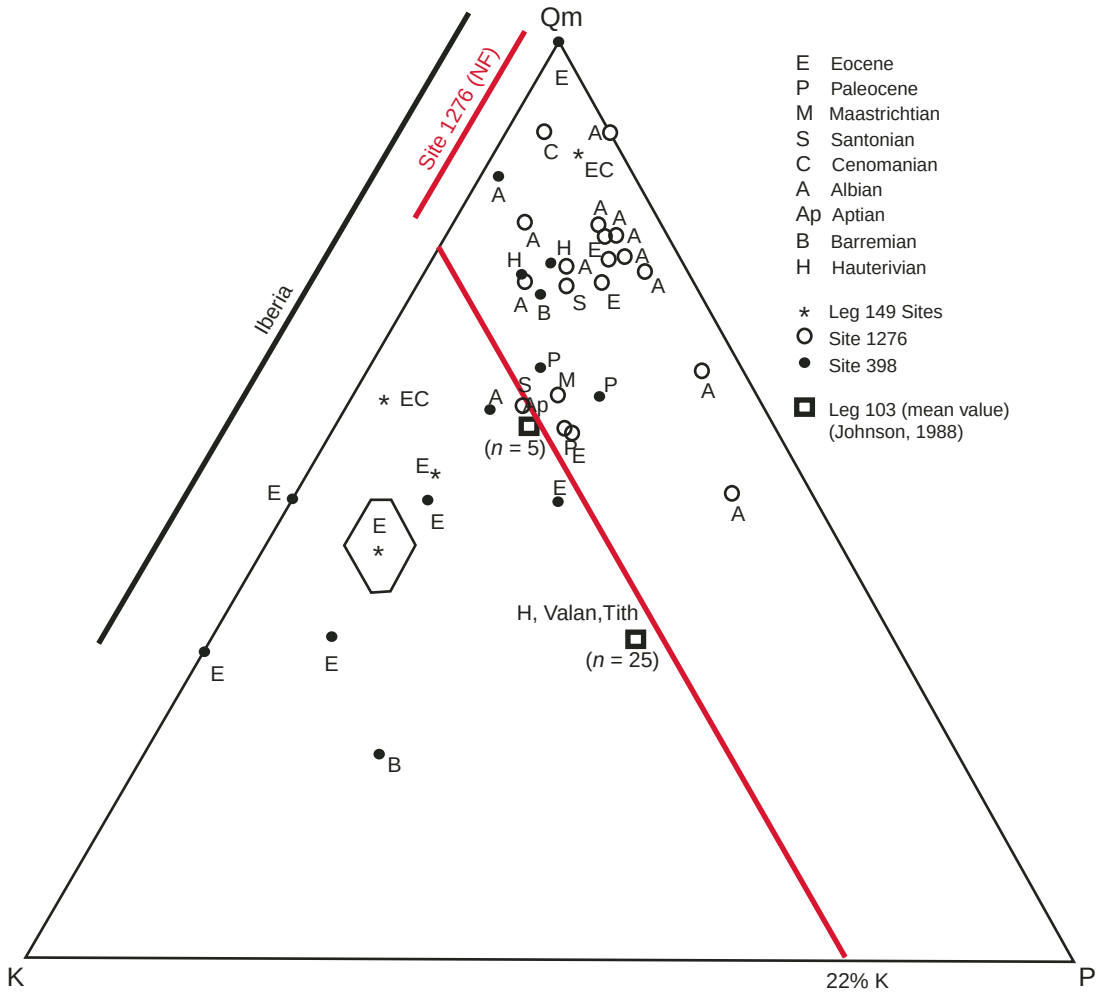

Figure F15. Ternary QFL plot of Lower Cretaceous sandstone data from Grand Banks and Iberian ODP and DSDP sites. Data for Site 398 are presented in Table T1, p. 38. Sources for other data as indicated. Note that L pole includes sedimentary carbonate lithic fragments.

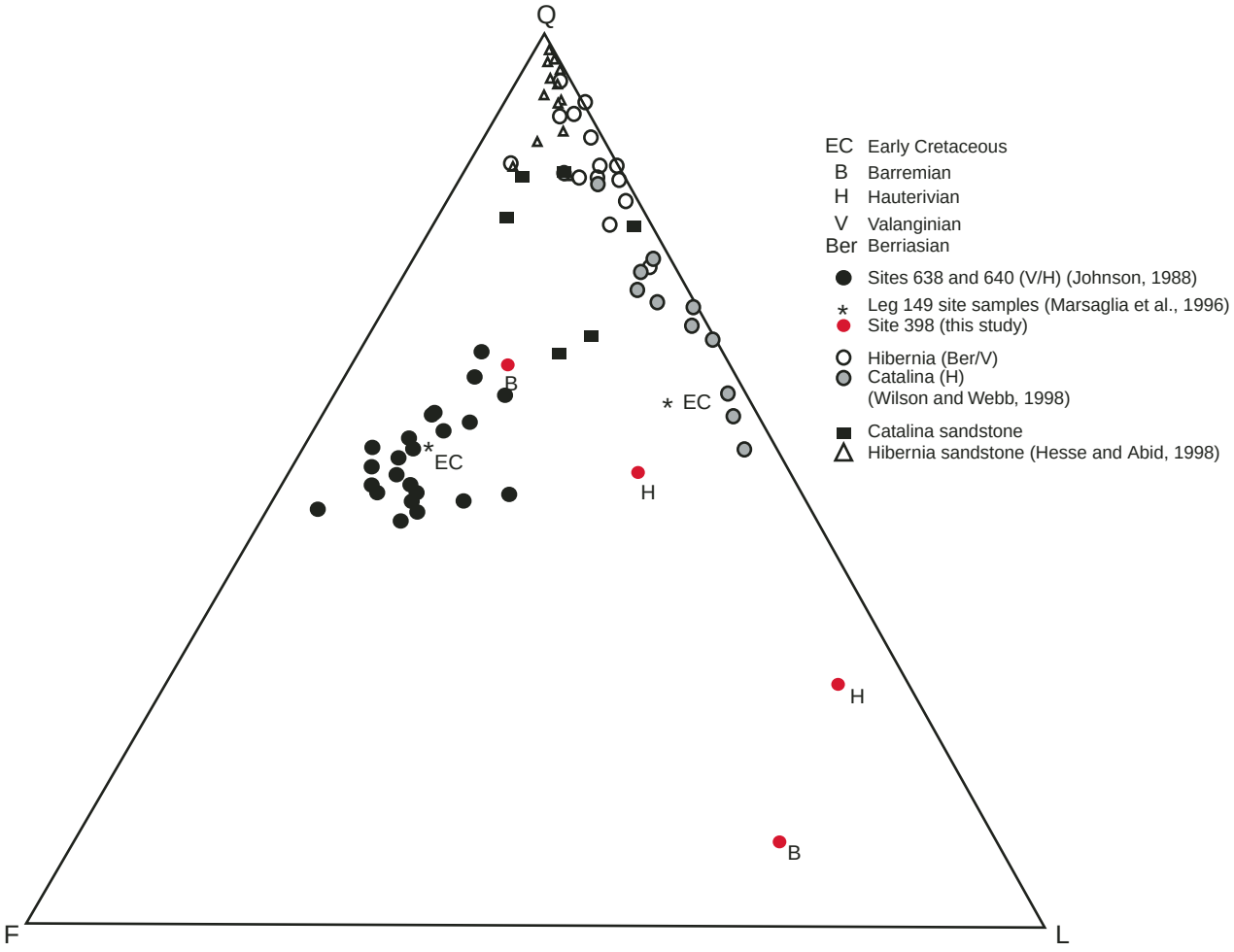

Figure F16. Ternary QFL plot of Tithonian and Jurassic sandstone data from Grand Banks and Iberian ODP sites. Data for Sites 1065 and 1069 are presented in Table T1, p. 38. Sources for other data as indicated. Note that L pole includes sedimentary carbonate lithic fragments.

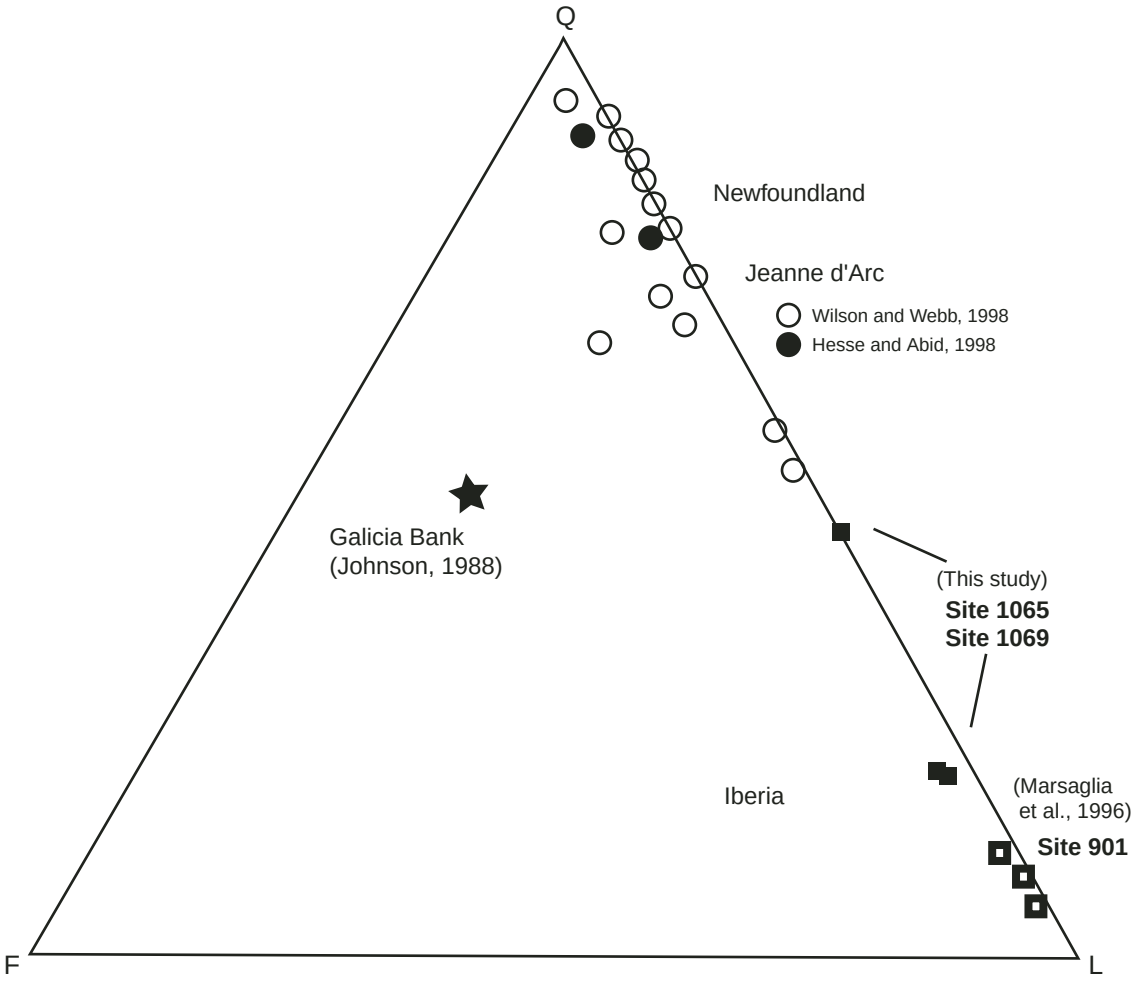

Figure F17. Tectonic terrane map of the Grand Banks and Iberian regions showing the position of the Hercynian Front and ODP Site 1276. Other geographical areas: NF = Newfoundland, FC = Flemish Cap, GS = Goban Spur, and GB = Galicia Bank. Numbered terranes: 1 = Cantabrian Zone, 2 = West-Asturian and Leonesian Zone, 3a + 3b = Central Iberian Zone, 4 = Ossa-Morena Zone, 5 = South Portugese Zone, and 6 = Rheno-Hercynian Zone. Other tectonic features include the Collector Anomaly suture zone (CA) and Porto-Badajoz-Cordoba suture (cbtl + psl + ptl). Modified from Capdevila and Mougenot (1988).

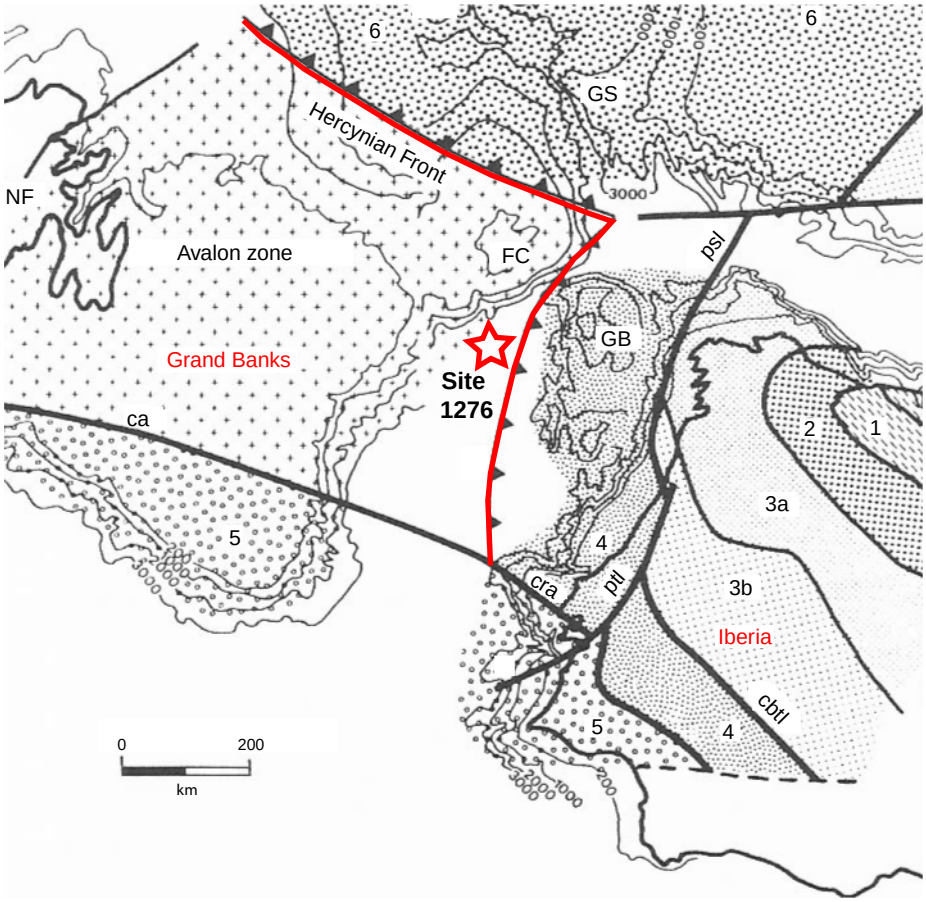

Figure F18. Rounded black tachylitic volcanic fragments with microlitic texture, and birefringent brown clay minerals (altered volcanic glass) (Sample 149-897C-62R-1, 123 cm). Porosity (blue) is likely a product of shrinkage of swelling clay minerals during thin section production. White areas (plane-polarized light) are where softer clay was gouged out during thin section preparation. **A.** Plane-polarized light. **B.** Cross-polarized light.

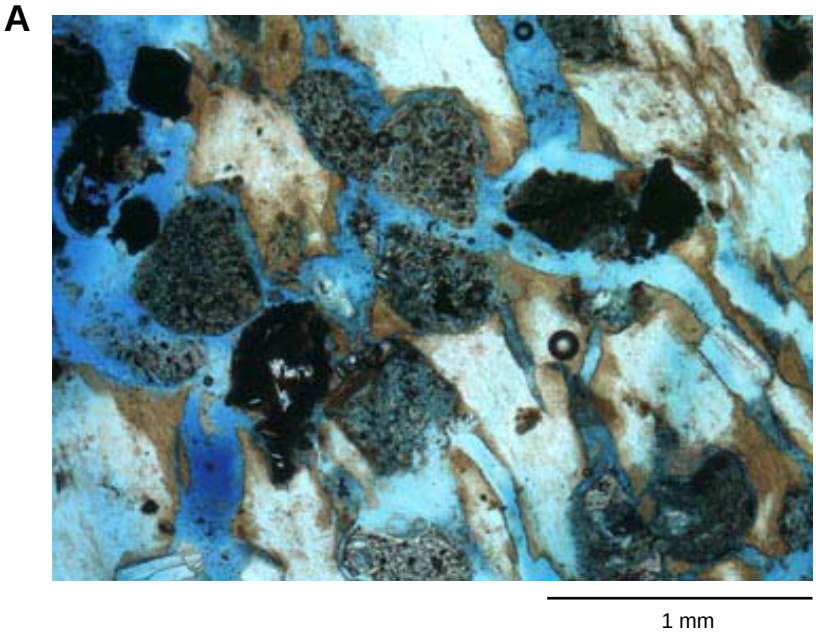

Figure F19. Angular brown to black (tachylitic) pyroclastic debris with local microlitic and vesicular textures (Sample 173-1068A-7R-2, 82 cm). A biotite fragment is present in the upper right corner of the field of view. These grains are set in a slightly birefringent matrix of clay minerals that could be altered fine ash. **A.** Plane-polarized light. **B.** Cross-polarized light.

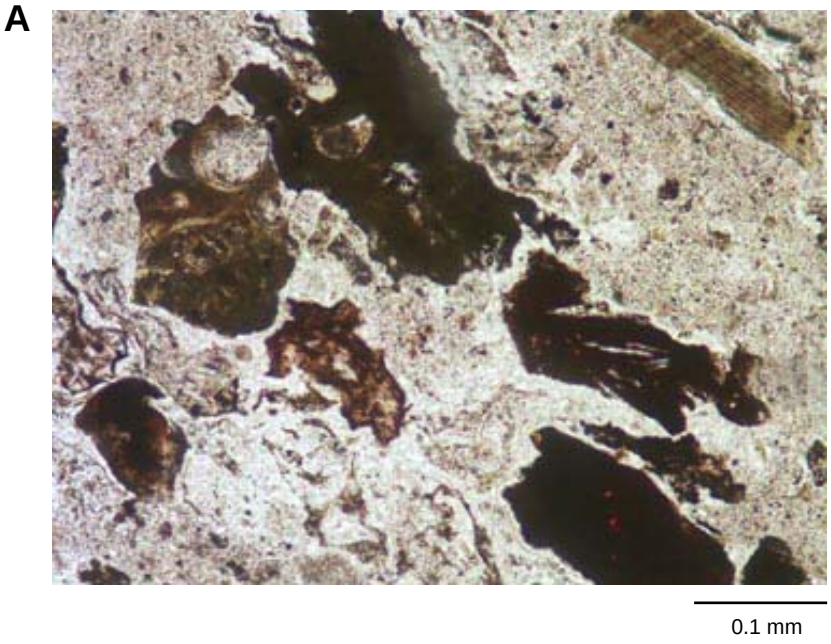

Figure F20. Sample 173-1069A-7R-2, 82 cm. **A.** Rounded altered microlitic volcanic fragment (plane-polarized light). **B.** Relict vesicular pumice textures (plane-polarized light). **C.** Relict vesicular pumice textures (cross-polarized light).

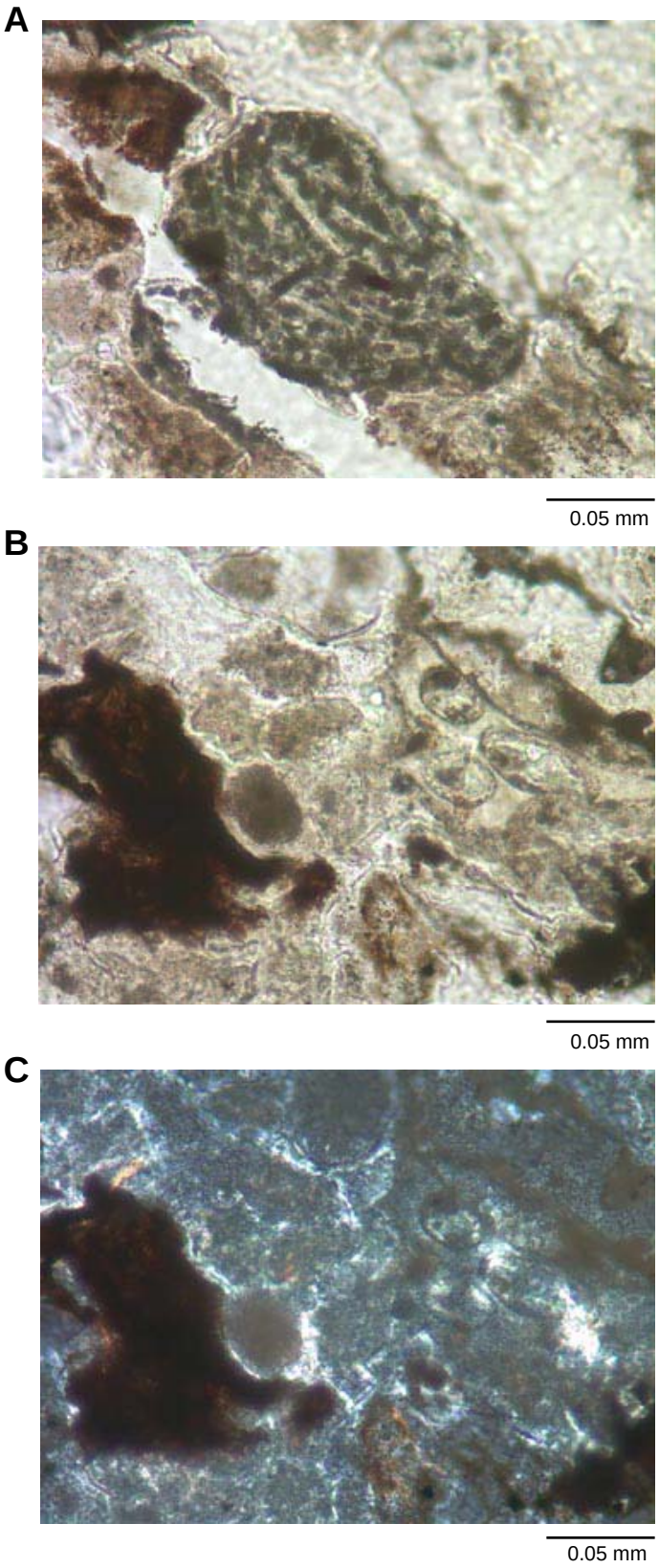

Figure F21. QFL plots showing distributions of rift and young ocean basin sand compositions and models for passive margin provenance. See text for discussion. **A.** Schematic summary of sand petrofacies outlined by Ingersoll (1990) within the modern Rio Grande Rift. **B.** Schematic summary of sand petrofacies (circled end members and mixing lines) within the Red Sea and Gulf of Aden, from Garzanti et al. (2001). **C.** Synthesis of modern data presented in A and B with Newfoundland/Iberian margin data used to expand undissected rift field. These exemplify ranges of sediment compositions possible in rift-to-drift settings. **D.** Schematic showing evolutionary paths that sand compositions may take within rift-to-drift successions. The arrows are labeled according to the type area on which they are based (e.g., Red Sea craton vs. volcanic based on Garzanti et al., 2001; Iberia based on data presented in Fig. F22, p. 37). Newfoundland example lacks arrow because trends uncertain. **E.** Conceptual rift-to-drift transition proposed by Dickinson (1985). Such compositional changes would be expected in mature rift stages in plutonic terranes with increased maturity (quartz content) as a function of enhanced weathering and transport.

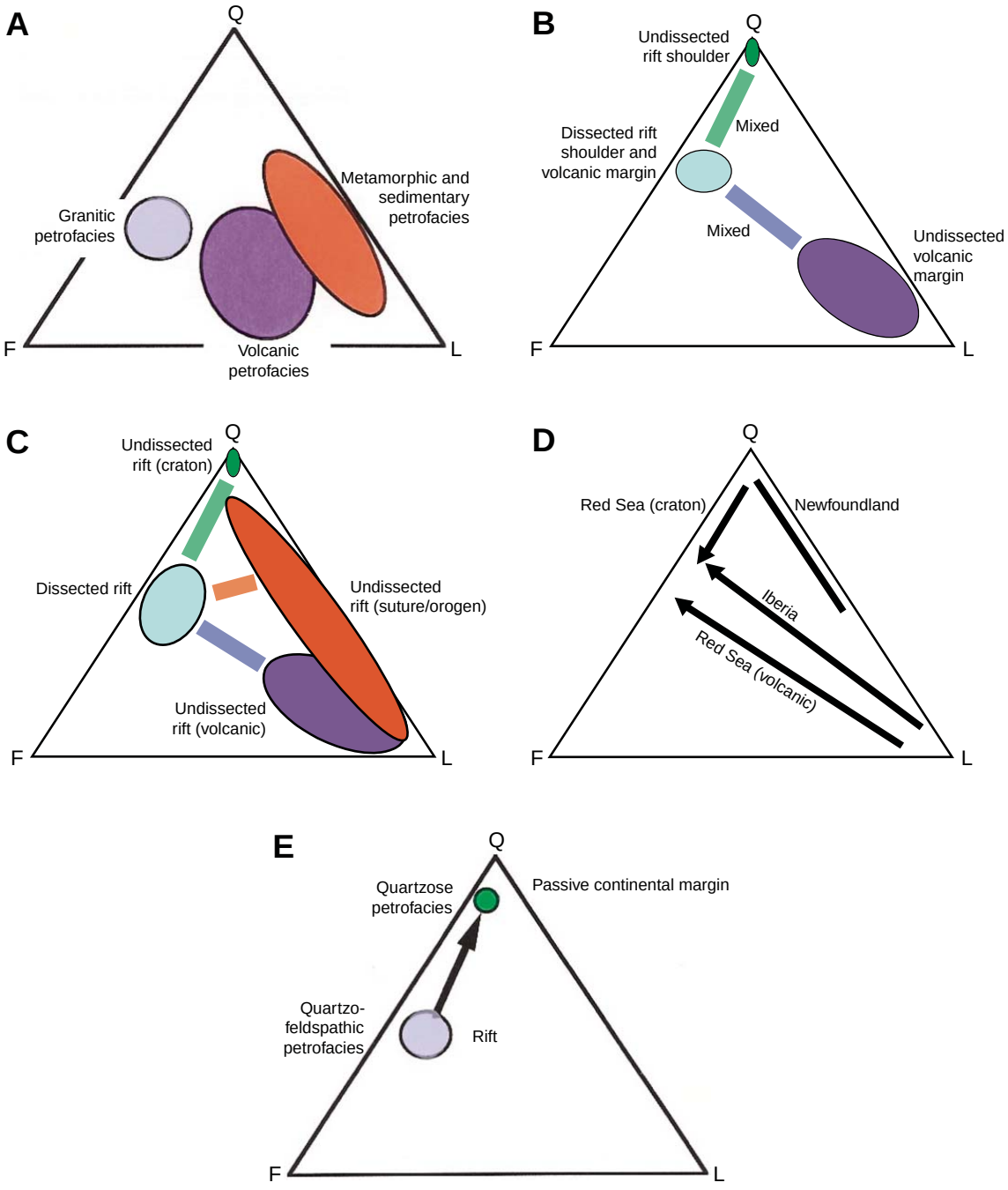

Figure F22. Paleogeographic reconstructions of Newfoundland–Iberian conjugate margins during the (**A**) early Tithonian and (**B**) Aptian after Boillot et al. (1989) showing the northward propagation of rifting from the Iberian/Newfoundland segment to the Galicia Bank/Flemish Cap segment. Schematic distributions of sand detrital modes on QFL plots for the (**C**) Galicia Bank segment and (**D**) Iberian segment show the temporal evolution in sand composition recorded at each site. Ternary plots based on data from Johnson (1988) in C and from Marsaglia et al. (1996) and this study in D. Note that rifting in both segments is characterized by lithic-rich sandstones.

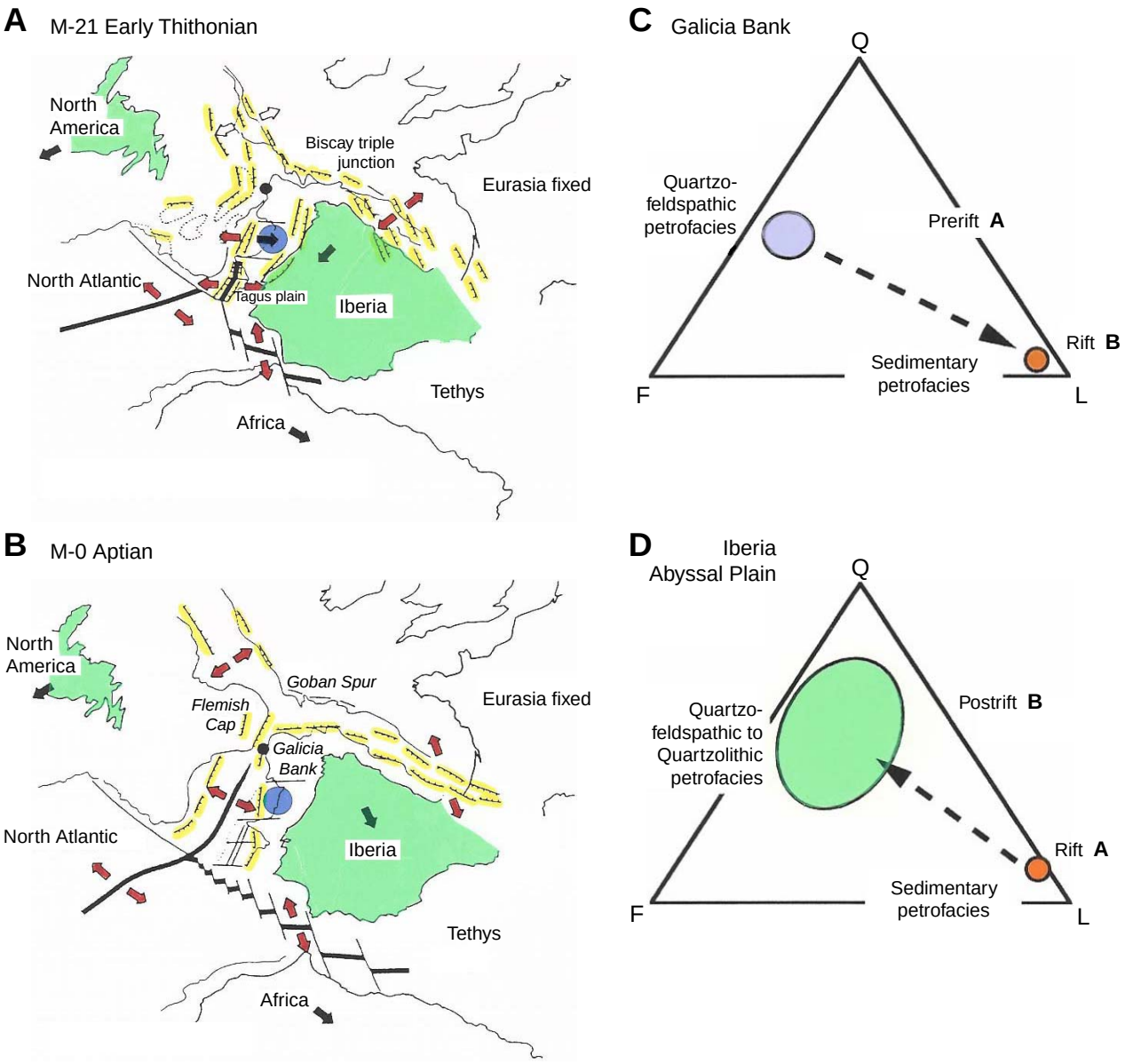

Table T1. Recalculated parameters based on data presented in Table AT1, p. 42. (See table notes. Continued on next three pages.)

Core, section, interval (cm)	Depth (mbsf)	Age	Unit	Average grain size	Sorting	Average rounding	QFL%Q	QFL%F	QFL%L	QmKP%Qm	QmKP%K	QmKP%P	P/F	LmLvLs %Lm	LmLvLs %Lv	LmLvLs %Ls	Ls%Lsc
47B-398-																	
21R-3, 63	607.10	Eocene		1	1	Subrounded	20	40	40	33.3	66.7	0	0	100	0	0	0
24R-3, 105	636.10	Eocene		2	3	Angular	26.8	22.5	50.7	50	37.5	12.5	0.25	18.2	0	81.8	66.7
26R-1, 43	651.40	Eocene		2	2	Subrounded	2.4	2.4	95.1	50	50	0	0	0	0	100	100
31R-2, 70	700.70	Eocene		2	2	Rounded	5.4	5.4	89.2	50	25	25	0.5	5.9	0	94.1	100
32R-3, 120	712.20	Eocene		3–4	2	Well rounded	9.1	0	90.9	100	0	0		20	0	80	87.5
36R-3, 124	750.24	Paleocene		2	2	Subrounded	27.3	14	58.7	64.3	19.6	16.1	0.45	12	1.2	86.7	86.1
40R-3, 8	787.08	Paleocene		1	2	Well rounded	21.1	13.2	65.8	61.5	15.4	23.1	0.6	12	0	88	86.4
104R-1, 66	1411.66	Albian		2	2	Angular	53.6	8	38.4	85.4	13.4	1.3	0.09	1.8	0	98.2	100
126R-2, 11	1621.61	Aptian		1	2	Subangular	44	29.9	26.1	59.3	27.1	13.6	0.33	67.3	0	32.7	75
127R-5, 62	1636.12	Barremain		2	2	Angular	63.5	21.9	14.6	72.6	15.5	11.9	0.43	47.4	0	52.6	25
128R-4, 0	1643.50	Barremain		2	3	Well rounded	9.4	21.9	68.8	22.2	55.6	22.2	0.29	15	0	85	76.5
134R-4, 33.5	1700.84	Hauterivian		3	3	Subrounded	26.8	7.1	66.1	76.5	11.8	11.8	0.5	38.2	0	61.8	100
137R-3, 89	1728.39	Hauterivian		1	1	Angular	51.1	15	33.8	74.7	16.5	8.9	0.35	37.1	0	62.9	95.5
210-1276A-																	
3R-4, 53	813.03	Eocene	1	2	1	Subangular	37.6	10.8	51.6	76.7	7	16.3	0.7	11.3	1.3	87.5	87.1
9R-2, 60	869.30	Eocene	2	3–4	3	Rounded	15.1	10.3	74.7	57.1	20	22.9	0.53	11.5	0	88.5	71
12R-4, 27	900.77	Eocene	2	2	2	Subrounded	43.1	13.9	43.1	74	9.1	16.9	0.65	17.5	14.3	68.3	81.4
15R-3, 46	928.46	Paleocene	2	2	1	Subrounded	9.6	10.5	79.9	46.3	26.8	26.8	0.5	2.1	0	97.9	87.4
						Average:	26.4	11.4	62.3	63.5	15.7	20.7	0.60	10.6	3.9	85.6	81.7
15R-4, 123	930.73	Paleocene	3	2	4	Angular	36.4	25.7	38	58.3	19.1	22.6	0.54	16.7	6.9	76.4	78.2
22R-1, 108	993.48	Maastrichtian	3	3	3	Subangular	45.1	26.6	28.2	61.5	19	19.5	0.51	14.9	9.2	75.9	37.9
25R-5, 92	1028.12	Santonian	4	2	1	Subangular	45.8	27.8	26.3	60.6	22	17.4	0.44	25	12.5	62.5	36.4
25R-6, 48	1029.28	Santonian	4	1	2	Subrounded	65	21.8	13.3	73.8	13.3	12.9	0.49	35.6	0	64.4	17.2
						Average:	48.1	25.5	26.5	63.6	18.4	18.1	0.50	23.1	7.2	69.8	42.4
35R-5, 120	1124.20	Cenomanian	5a	2	2	Subrounded	83.9	9.1	7	89.9	6.3	3.7	0.37	23.3	3.3	73.3	40.9
44R-2, 129	1205.99	Albian	5b	1	1	Subrounded	62.5	18.6	18.9	76.3	11.8	11.8	0.5	28.4	0	71.6	4.2
49R-2, 130	1254.20	Albian	5b	1	1	Angular	57.9	18.7	23.4	75.2	4.7	20.1	0.81	53.8	9	37.2	41.4
56R-3, 65	1322.45	Albian	5b	2	3	Angular	72.4	6.8	20.7	90.4	0	9.6	1	29.5	1.3	69.2	59.3
65R-5, 6	1407.86	Albian	5b	1	1	Angular	43.3	36.8	19.8	50.8	7.6	41.7	0.85	56.4	7.7	35.9	53.6
69R-4, 86	1445.16	Albian	5b	1	1	Subangular	49.7	27.2	23	63.5	3.8	32.7	0.9	34.6	1.2	64.2	46.2
73R-2, 87	1480.90	Albian	5b	1	1	Subangular	60.1	13.7	26.3	80.4	6.3	13.3	0.68	40	0	60	6.7
						Average:	57.7	20.3	22.0	72.8	5.7	21.5	0.79	40.5	3.2	56.4	35.2
80R-3, 107	1549.87	Albian	5c	1	2	Subangular	74	16.4	9.5	80.9	5.6	13.6	0.71	45.5	0	54.5	33.3
81R-3, 134	1559.74	Albian	5c	1–2	3	Angular	65.5	16.2	18.4	78.6	5.5	15.9	0.74	58.6	0	41.4	33.3
87R-4, 0	1609.00	Albian	5c	3	4	Angular	65	15.5	19.4	78.3	11.2	10.5	0.48	29.7	0	70.3	23.1
90R-5, 87	1620.97	Albian	5c	2–3	3	Angular	60.2	13.7	26.1	80.4	6.3	13.3	0.68	39	0	61	8.2
93R-1, 24	1662.34	late Aptian–early Albian	5c	3	3	Subangular	62.5	15.1	22.4	79.3	5.9	14.8	0.71	30.1	0	69.9	27.6
96R-1, 127	1692.17	late Aptian–early Albian	5c	2	1	Subangular	61.1	16.3	22.6	76.7	5.4	17.8	0.77	55.4	6	38.6	37.5
						Average:	64.7	15.5	19.7	79.0	6.7	14.3	0.68	43.1	1.0	56.0	27.2

Table T1 (continued).

Core, section, interval (cm)	Depth (mbsf)	Age	Unit	Average grain size	Sorting	Average rounding	Total grains		Total %		Lm+M			M%		
							%Bioclasts	%Mica	Porosity	Cement	%Biotite	%Muscovite	%Chlorite	Biotite	Muscovite	Chlorite
47B-398-																
21R-3, 63	607.10	Eocene		1	1	Subrounded	68.2	4.5	1.3	0						
24R-3, 105	636.10	Eocene		2	3	Angular	32.3	3.2	2.3	0						
26R-1, 43	651.40	Eocene		2	2	Subrounded	94.7	1.1	4.3	0						
31R-2, 70	700.70	Eocene		2	2	Rounded	95	0	10	0						
32R-3, 120	712.20	Eocene		3–4	2	Well rounded	92.2	0	5	1						
36R-3, 124	750.24	Paleocene		2	2	Subrounded	60.3	0	6.9	15.7						
40R-3, 8	787.08	Paleocene		1	2	Well rounded	77.7	1.1	7	2						
104R-1, 66	1411.66	Albian		2	2	Angular	1.6	1	0.4	33.9						
126R-2, 11	1621.61	Aptian		1	2	Subangular	0.7	11.9	0	42.5						
127R-5, 62	1636.12	Barremain		2	2	Angular	0.3	4.4	0	0						
128R-4, 0	1643.50	Barremain		2	3	Well rounded	0	16	0	3						
134R-4, 33.5	1700.84	Hauterivian		3	3	Subrounded	7.3	7.3	1.3	2.7						
137R-3, 89	1728.39	Hauterivian		1	1	Angular	0.8	9	0	40.3						
210-1276A-																
3R-4, 53	813.03	Eocene	1	2	1	Subangular	66.8	3	15.7	7.9	68.4	26.3	5.3	66.7	33.3	0.0
9R-2, 60	869.30	Eocene	2	3–4	3	Rounded	34	0.4	1.2	1.2	50.0	50.0	0.0	0.0	100.0	0.0
12R-4, 27	900.77	Eocene	2	2	2	Subrounded	54.5	1.4	1.9	73.1	31.3	26.3	31.3	27.3	54.5	18.2
15R-3, 46	928.46	Paleocene	2	2	1	Subrounded	62.8	0.4	13	2.4	59.3	37.0	3.7	25.0	62.5	12.5
						Average:	54.5	1.3	8.0	21.2						
15R-4, 123	930.73	Paleocene	3	2	4	Angular	2.9	11	1.8	0.8	33.3	66.7	0.0	50.0	50.0	0.0
22R-1, 108	993.48	Maastrichtian	3	3	3	Subangular	14.2	1.3	3.1	25.5	66.7	33.3	0.0	25.0	75.0	0.0
25R-5, 92	1028.12	Santonian	4	2	1	Subangular	9.7	1.6	2.8	40.5	26.9	65.4	7.7	19.0	76.2	4.8
25R-6, 48	1029.28	Santonian	4	1	2	Subrounded	0	3.8	9.9	10.1	65.4	3.8	30.8	54.5	0.0	45.5
						Average:	6.7	4.4	4.4	19.2						
35R-5, 120	1124.20	Cenomanian	5a	2	2	Subrounded	0.5	0.8	1.3	37.7	60.0	20.0	20.0	50.0	0.0	50.0
44R-2, 129	1205.99	Albian	5b	1	1	Subrounded	0.8	4.3	12.9	1.4	33.3	29.2	37.5	11.1	22.2	66.7
49R-2, 130	1254.20	Albian	5b	1	1	Angular	1.5	0	2	0	45.7	48.6	5.7	45.7	48.6	5.7
56R-3, 65	1322.45	Albian	5b	2	3	Angular	8.2	4.7	5.8	0	48.1	48.1	3.7	18.2	81.8	0.0
65R-5, 6	1407.86	Albian	5b	1	1	Angular	2.9	5.2	2	0	52.8	43.4	3.8	42.4	57.6	0.0
69R-4, 86	1445.16	Albian	5b	1	1	Subangular	3.7	4.5	2.7	40.8	59.0	15.4	25.6	68.2	9.1	22.7
73R-2, 87	1480.90	Albian	5b	1	1	Subangular	0.5	1.3	4.2	40.7	36.8	26.3	36.8	39.4	27.3	33.3
						Average:	2.9	3.3	4.9	13.8						
80R-3, 107	1549.87	Albian	5c	1	2	Subangular	0	3.6	0.1	39.4	25.0	25.0	50.0	66.7	0.0	77.8
81R-3, 134	1559.74	Albian	5c	1–2	3	Angular	0.3	7.3	0.2	64.1	40.8	28.6	30.6	23.8	23.8	52.4
87R-4, 0	1609.00	Albian	5c	3	4	Angular	0	1.8	1.8	22.6	27.8	38.9	33.3	0.0	45.5	54.5
90R-5, 87	1620.97	Albian	5c	2–3	3	Angular	0.5	1.3	4.5	42.5	36.8	26.3	36.8	39.4	27.3	33.3
93R-1, 24	1662.34	late Aptian–early Albian	5c	3	3	Subangular	2.3	2.6	2.7	37.7	41.4	44.8	13.8	21.1	68.4	10.5
96R-1, 127	1692.17	late Aptian–early Albian	5c	2	1	Subangular	0	2.1	0	46.7	41.3	39.1	19.6	44.7	34.2	21.1
						Average:	0.5	3.1	1.6	42.2						

Table T1 (continued).

Core, section, interval (cm)	Depth (mbsf)	Age	Unit	Average grain size	Sorting	Average rounding	QFL%Q	QFL%F	QFL%L	QmKP%Qm	QmKP%K	QmKP%P	P/F	LmLvLs %Lm	LmLvLs %Lv	LmLvLs %Ls	Ls%Lsc
173-1069A-																	
15R-1, 38		Campanian					52.6	17.3	30.1	82.7	8.4	8.9	0.52	33.3	0	66.7	93.9
17R-1, 98		Late Jurassic					19.6	2.2	78.3	100	0	0		91.7	0	8.3	33.3
173-1065A-																	
8R-CC, 8		Tithonian					20.9	2.1	77	92.2	1.3	6.5	0.83	55.3	0	44.7	69.2
22R-CC, 16		Mid/Late Jurassic					45.6	0	54.4	100	0	0		75.8	0	24.2	45.8

Notes: Average grain size: 1 = very fine; 2 = fine; 3 = medium; 4 = coarse; 5 = very coarse. Sorting: 1 = well sorted; 2 = moderately sorted; 3 = poorly sorted; 4 = very poorly sorted. Q = total monocrystalline and polycrystalline quartz; F = Total plagioclase and potassium feldspar; L = total Lithic fragments including carbonate lithic fragments. Qm = monocrystalline quartz; K = potassium feldspar; P = plagioclase feldspar. Lm = metamorphic lithics; Ls = sedimentary lithics; Lv = volcanic lithics; Lsc = sedimentary carbonate lithics. Mica includes muscovite, biotite and chlorite. %Biotite bearing metamorphic (Lm) and mica (M) clasts. %Muscovite bearing metamorphic (Lm) and mica (M) clasts. %Chlorite bearing metamorphic (Lm) and mica (M) clasts.

Table T1 (continued).

Core, section, interval (cm)	Depth (mbsf)	Age	Unit	Average grain size	Sorting	Average rounding	Total grains		Total %		Lm+M			M%		
							%Bioclasts	%Mica	Porosity	Cement	%Biotite	%Muscovite	%Chlorite	Biotite	Muscovite	Chlorite
173-1069A-																
15R-1, 38		Campanian					11.6	0.3	0.3	41.5						
17R-1, 98		Late Jurassic					0	2.2	0	66.3						
173-1065A-																
8R-CC, 8		Tithonian					8.8	1.6	0.2	23.9						
22R-CC, 16		Mid/Late Jurassic					11.2	0	0	49.2						

Table AT1. Point-count categories.

Category	Definition
Qp	Polycrystalline quartz
Qm	Monocrystalline quartz
P	Plagioclase feldspar
K	Potassium feldspar
F(?)	Feldspar (?) (possible feldspar-unstained thin section)
Lmm	Polycrystalline mica lithic (mixed or undetermined mica mineralogy)
Lmm-b	Polycrystalline mica lithic with biotite
Lmm-m	Polycrystalline mica lithic with muscovite
Lmm-c	Polycrystalline mica lithic with chlorite
Lmt	Quartz-mica tectonite lithic (mixed or undetermined mica mineralogy)
Lmt-b	Quartz-mica tectonite lithic with biotite
Lmt-m	Quartz-mica tectonite lithic with muscovite
Lmt-c	Quartz-mica tectonite lithic with chlorite
Lmt-alt	Quartz-mica tectonite lithic–altered
Lma	Quartz-feldspar-mica aggregate lithic (mixed or undetermined mica mineralogy)
Lma-b	Quartz-feldspar-mica aggregate lithic with biotite
Lma-m	Quartz-feldspar-mica aggregate lithic with muscovite
Lma-c	Quartz-feldspar-mica aggregate lithic with chlorite
Lmp	Metapelite lithic fragments
Lmc	Metacarbonate lithic fragments
Lsp	Sandy siltstone lithic fragment with detrital micas
Lsch	Sedimentary chert or cherty claystone lithic
Lsa	Claystone-shale lithic
Lsa A/D	Partially dissolved or altered claystone-shale lithic
Lsc micr	Microcrystalline calcite clasts
Lsc micr A/D	Altered/partially dissolved micrite clast
Lsc carb	Carbonate lithic clast
Unk Carb	Carbonate clast of unknown origin
Lv	Volcanic lithic
Op	Opaque dense minerals
Non-op	Nonopaque dense minerals
Biot	Biotite
Biot alt chl	Biotite altering to chlorite
Mu	Muscovite
Chl	Chlorite
Glauc	Glauconite
Other/unk	Other/Unknown grain
P-foram	Planktonic foraminifers
B-foram	Benthic foraminifers
Other foram	Foraminifer of unknown type or altered/dissolved
Sponge sp	Sponge spicule
Bryoz	Bryozoan
Red alg	Red algae
Rad	Radiolarian
Mollusk	Mollusk
Echino	Echinoderm
Ost	Ostracode
Bone frag	Bone fragment or other phosphatic fish debris
Pl	Plant (organic) matter
Bio other	Other or unknown bioclastic debris
Matrix silt	Silt matrix
Matrix clay	Clay matrix
matrix micrite	Micrite matrix
Other matrix	Other matrix
Carb cmt	Carbonate cement
Micr cmt	Micritic carbonate cement
Silica cmt	Quartz overgrowth cement
Gyp cmt	Gypsum cement
Zeol cmt	Zeolite cement
Op cmt	Opaque cement
Micro clay	Microporous clay
P intra	Intraparticle porosity
P inter	Interparticle porosity
P intra dissol	Secondary porosity due to dissolution of detrital grains
P frac	Fracture porosity
P other	Porosity of other/unknown origin

Table AT2. Point-count data collected for this study. (Continued on next three pages.)

Core, section, interval (cm)	Depth (mbsf)	Age	Qm	Qp	P	K	F(?)	Lmm	Lmm-b	Lmm-m	Lmm-c	Lmt	Lmt-b	Lmt-m	Lmt-c	Lmt alt	Lma	Lma-b	Lma-c	Lma-m	Lmp	Lmc
47B-398-																						
21R-3, 63	607.10	Eocene	1			2			1			1										
24R-3, 105	636.10	Eocene	16	3	4	12		3				4					2					
26R-1, 43	651.40	Eocene	1			1																
31R-2, 70	700.70	Eocene	2		1	1			1				1									
32R-3, 120	712.20	Eocene	2									4										
36R-3, 124	750.24	Paleocene	36	3	9	11		1	1	1		4	1	2			1					
40R-3, 8	787.08	Paleocene	8		3	2						3										
104R-1, 66	1411.66	Albian	134	21	2	21		1			1				1							
126R-2, 11	1621.61	Aptian	105	1	24	48		14	3	4	5	7	1	3	8			1		1		
127R-5, 62	1636.12	Barremain	159	15	26	34		2		4	3	2	2	1	1		5					
128R-4, 0	1643.50	Barremain	2	1	2	5		2				2				1						
134R-4, 33.5	1700.84	Hauterivian	13	2	2	2		3	2			6	1		1		3					
137R-3, 89	1728.39	Hauterivian	59	9	7	13		10				9					4					
173-1069A-																						
15R-4, 38		Campanian	148	25	16	15	26			3		1	9	3			2	1		4	8	2
17R-1, 98		Late Jurassic	9				1			2		1		14						6	10	
173-1065A-																						
8R-CC, 8		Tithonian	71		5	1	1		1	4	1	11	3	58	5		1			2	58	1
22R-CC, 16		Mid/Late Jurassic	74	9						1				22						2	50	
210-1276A-																						
3R-4, 53	813.03	Eocene	33	2	7	3			6	2				1								
9R-2, 60	869.30	Eocene	40	4	16	14								1							24	
12R-4, 27	900.77	Eocene	57	5	13	7			2	1			1	4	1				1	1		
15R-4, 123	930.73	Paleocene	67	1	26	22				3	1	2	2	1						1	2	
15R-3, 46	928.46	Paleocene	19	1	11	11						1					1	1		1		
22R-1, 108	993.48	Maastrichtian	136	8	43	42		3				2	1				6			3	1	
25R-5, 92	1028.12	Santonian	143	10	41	52				1			2	10	1		1	2		5		
25R-6, 48	1029.28	Santonian	217	13	38	39		2	1		2	1	3		2	2	2	2	1			
35R-5, 120	1124.20	Cenomanian	313	11	13	22			1			5			1							
44R-2, 129	1205.99	Albian	219	9	34	34		2			1	8	1	2	5		2					
49R-2, 130	1254.20	Albian	191	4	51	12		1	3	3		2	11	11	2	5		2		3		
56R-3, 65	1322.45	Albian	206	28	22				1	3		4	1	5			2			1	6	
65R-5, 6	1407.86	Albian	134	19	110	20			5	4		7	8	11		4		1		4		
69R-4, 86	1445.16	Albian	169	8	87	10		1	6		3	2	9	2	2		1				3	
73R-2, 87	1480.90	Albian	217	16	36	17		2	5	1	4	5	8	8	6		2		1			
80R-3, 107	1549.87	Albian	262	17	44	18		3			3	3	2		4		1				2	
81R-3, 134	1559.74	Albian	213	22	43	15		8	4	2	5	11	1	3	6		2					
87R-4, 0	1609.00	Albian	217	34	29	31		1				7		4	6		3			1	1	
90R-5, 87	1620.97	Albian	217	16	36	17		2	5	1	4	4	8	8	6		2		1			
93R-1, 24	1662.34	late Aptian–early Albian	214	18	40	16				3	1	4	4	9	1		1			1		1
96R-1, 127	1692.17	late Aptian–early Albian	198	27	46	14			5		2	5	12	13	6	1	2					

Note: See Table AT1, p. 42, for definitions of point-count categories.

Table AT2 (continued).

Core, section, interval (cm)	Depth (mbsf)	Age	Lsp	Lsch	Lsa	Lsa A/D	Lsc micr	Lsc micr A/D	Lsc carb	Unk carb	Lv	Op	Non-Op	Biot	Biot alt chl	Mu	Chl	Glauc	Other/ unk	P-foram	B-Foram	Other foram	Sponge sp
47B-398-																							
21R-3, 63	607.10	Eocene										1			1							0	2
24R-3, 105	636.10	Eocene			9		5		13			2		1		2			3	10		9	3
26R-1, 43	651.40	Eocene					30		9					1					5	60		29	1
31R-2, 70	700.70	Eocene					21	4	7			1							2	120	2	27	
32R-3, 120	712.20	Eocene			2		11		9	1									0	82	1	9	
36R-3, 124	750.24	Paleocene			10		8		54		1	1	1					4		120	1	7	
40R-3, 8	787.08	Paleocene			3				19								1			36	1	35	
104R-1, 66	1411.66	Albian					85		16	7		3	1			2		1		3		0	
126R-2, 11	1621.61	Aptian			4		7		5			18	2	18		16			2	1		1	
127R-5, 62	1636.12	Barremain			15		4		1			7	4	2		10	1	1				0	
128R-4, 0	1643.50	Barremain	2		2		6		8					1		3			5			0	
134R-4, 33.5	1700.84	Hauterivian					5		16					3					2			1	
137R-3, 89	1728.39	Hauterivian			1		15		6			7		3		7	2		5			0	
173-1069A-																							
15R-4, 38		Campanian	3		1		54		8					1					5	2	1	11	
17R-1, 98		Late Jurassic			2				1							1			3			0	
173-1065A-																							
8R-CC, 8		Tithonian	24		12		75		6			23	2		1	4						10	
22R-CC, 16		Mid/Late Jurassic	9		4		6		5			3										0	
210-1276A-																							
3R-4, 53	813.03	Eocene		4	5	2	11		50		1	16	1	7		2	1	12	2	113	13	17	1
9R-2, 60	869.30	Eocene	56				61		76				6	1				4	7	8	45	9	
12R-4, 27	900.77	Eocene			8		4	7	10		9	5	6	2			3	30	2	117	23	4	
15R-4, 123	930.73	Paleocene	5		7		40		3		5	3		14		5			6	3		0	2
15R-3, 46	928.46	Paleocene	5		19		45	32	90				2			1		13		13	16	13	
22R-1, 108	993.48	Maastrichtian	10		31		19	5	1		8	5		5				11	2	28	1	14	
25R-5, 92	1028.12	Santonian	26	2	7		2	17			11	5		3	1	1	1	18		1		3	1
25R-6, 48	1029.28	Santonian	24				2	2	1				5	11		1	3	25	1			0	
35R-5, 120	1124.20	Cenomanian	10		3			3	6		1	2	1	2		1			1	1		0	
44R-2, 129	1205.99	Albian	38		8		1	1				7	5	7	2	5	3	1	2	3		0	
49R-2, 130	1254.20	Albian			17	13	3	7	2		7								3	3		0	
56R-3, 65	1322.45	Albian	12		10		4	12	16		1	14		11	1	4	1	1	3	3		0	
65R-5, 6	1407.86	Albian		1	12		2		13		6	4	3	14		4	2	1		3		1	
69R-4, 86	1445.16	Albian		3	25		9	14	1		1	10	5	8		4	5	1		6		1	
73R-2, 87	1480.90	Albian		2	54		2		2			5		1		1	3					0	
80R-3, 107	1549.87	Albian	12				5		1			5	3	3	3	5	3		1			0	
81R-3, 134	1559.74	Albian			16		7		1			3	2	15		9	4		7	1		0	
87R-4, 0	1609.00	Albian	36	1	3		9		3			3		5		2			3			0	
90R-5, 87	1620.97	Albian		2	54		2		3			5		1		1	3					0	
93R-1, 24	1662.34	late Aptian–early Albian		4	38		12		4			7	1	8			2					0	
96R-1, 127	1692.17	late Aptian–early Albian			20		3		9		5	15	3	2		5	1		5			0	

Table AT2 (continued).

Core, section, interval (cm)	Depth (mbsf)	Age	Bryoz	Red alg	Rad	Mollusk	Echino	Ost	Bone Frag	Pl	Bio other	Total grains	Matrix silt	Matrix clay	Matrix micrite	Other matrix	Carb cmt	Micr cmt	Silica cmt	Gyp cmt	Zeol cmt	Op cmt	Micro clay
47B-398-																							
21R-3, 63	607.10	Eocene			13							22	272	2									2
24R-3, 105	636.10	Eocene	1	1	3	3					5	114	11	38	114								16
26R-1, 43	651.40	Eocene									2	139	19	23	38								68
31R-2, 70	700.70	Eocene	1	1							1	193	22	1	16			3					15
32R-3, 120	712.20	Eocene				1		1				123	27	17	82	2	3						9
36R-3, 124	750.24	Paleocene	1			3						281			44		40	20		6			
40R-3, 8	787.08	Paleocene						1			1	113	16	3	93		6	5					42
104R-1, 66	1411.66	Albian								1		300	2	3	12		132	32					
126R-2, 11	1621.61	Aptian									1	300	102	30	6		310	15					1
127R-5, 62	1636.12	Barremain				1						300											
128R-4, 0	1643.50	Barremain									2	44	24	15	203		9						
134R-4, 33.5	1700.84	Hauterivian				2						64	32	47	140	2	4	4					1
137R-3, 89	1728.39	Hauterivian				1					1	159	19			2	117	3					
173-1069A-																							
15R-4, 38		Campanian				6	15					370					264						
17R-1, 98		Late Jurassic										50	11				104	16					
173-1065A-																							
8R-CC, 8		Tithonian				4	14			3		401				179	108	6				12	
22R-CC, 16		Mid/Late Jurassic					22					207	21	5			203	21				2	
210-1276A-																							
3R-4, 53	813.03	Eocene	13	1	18	42	4	3	3		4	400					26	13	19	9			
9R-2, 60	869.30	Eocene	5		2	12	6				3	400	34	39	245	6	1	8					38
12R-4, 27	900.77	Eocene	4			46	1		5		2	381	1			121	1172				4	2	5
15R-4, 123	930.73	Paleocene										221	313		289		5	1		1	22		36
15R-3, 46	928.46	Paleocene		2		23	78					400	18	107	31	3	14						
22R-1, 108	993.48	Maastrichtian				5	5				5	400	25	15	19	2	148	16					3
25R-5, 92	1028.12	Santonian				2	30					399				11	274						
25R-6, 48	1029.28	Santonian										400	81	34			57		10	2			35
35R-5, 120	1124.20	Cenomanian				1					2	400	48	17	1		276	13					8
44R-2, 129	1205.99	Albian										400	107	62			1		9				57
49R-2, 130	1254.20	Albian	1		1							358											
56R-3, 65	1322.45	Albian				8	19			1		400				1							
65R-5, 6	1407.86	Albian	4			3						400											
69R-4, 86	1445.16	Albian				7						403			70	70	320	8				4	
73R-2, 87	1480.90	Albian				2						400	36				317	8		1		4	10
80R-3, 107	1549.87	Albian										400	58	16			252	62	3				12
81R-3, 134	1559.74	Albian										400				126	697	19				1	
87R-4, 0	1609.00	Albian									1	400	80	13			146	3				5	21
90R-5, 87	1620.97	Albian				2						400	2			44	317	8				4	10
93R-1, 24	1662.34	late Aptian–early Albian	1			5	3			2		400	7			46	231	32			1	6	
96R-1, 127	1692.17	late Aptian–early Albian									1	400				32	349					2	

Table AT2 (continued).

Core, section, interval (cm)	Depth (mbsf)	Age	P intra	P inter	P intra dissol	P frac	P other	Total pts
47B-398-								
21R-3, 63	607.10	Eocene	2					322
24R-3, 105	636.10	Eocene	7					414
26R-1, 43	651.40	Eocene	10	3				439
31R-2, 70	700.70	Eocene	15	7	28			493
32R-3, 120	712.20	Eocene	15		22			423
36R-3, 124	750.24	Paleocene	25	3	1			701
40R-3, 8	787.08	Paleocene	18	3	1			413
104R-1, 66	1411.66	Albian				1	2	784
126R-2, 11	1621.61	Aptian						1064
127R-5, 62	1636.12	Barremain						600
128R-4, 0	1643.50	Barremain				5		344
134R-4, 33.5	1700.84	Hauterivian			4	2		364
137R-3, 89	1728.39	Hauterivian						459
173-1069A-								
15R-4, 38		Campanian	1		1			1006
17R-1, 98		Late Jurassic						231
173-1065A-								
8R-CC, 8		Tithonian						1107
22R-CC, 16		Mid/Late Jurassic						666
210-1276A-								
3R-4, 53	813.03	Eocene	19		30			916
9R-2, 60	869.30	Eocene	1	6	2	3		1183
12R-4, 27	900.77	Eocene	5		17			2089
15R-4, 123	930.73	Paleocene		3	12			1124
15R-3, 46	928.46	Paleocene	2	6	8			987
22R-1, 108	993.48	Maastrichtian	3		12	1		1044
25R-5, 92	1028.12	Santonian			2			1085
25R-6, 48	1029.28	Santonian		58	8	1		1086
35R-5, 120	1124.20	Cenomanian	1	2	1			1167
44R-2, 129	1205.99	Albian	6	68	19			1129
49R-2, 130	1254.20	Albian						716
56R-3, 65	1322.45	Albian						801
65R-5, 6	1407.86	Albian						800
69R-4, 86	1445.16	Albian			8			1286
73R-2, 87	1480.90	Albian			34			1210
80R-3, 107	1549.87	Albian			1			1204
81R-3, 134	1559.74	Albian			2			1645
87R-4, 0	1609.00	Albian		4	8	1		1081
90R-5, 87	1620.97	Albian			34			1219
93R-1, 24	1662.34	late Aptian–early Albian			2		17	1142
96R-1, 127	1692.17	late Aptian–early Albian						1183

CHAPTER NOTES*

N1. Wilson, M.D., and Webb, J.C., 1998. Reservoir quality of Jurassic and Cretaceous sandstones in ten wells Grand Banks area, offshore Canada, unpublished report.

N2. Georgescu, M.D., Leckie, R.M., and Hiscott, R.N., submitted. Latest Paleocene and Early Eocene large-sized reworked benthic foraminifers in the Newfoundland Basin (Ocean Drilling Program Leg 210, Site 1276) and their paleoclimate significance. *Rev. Micropaleontol*.

*Dates reflect file corrections or revisions.